Evidence for Josephson vortices in $(BEDT\text{-}TTF)_2Cu(NCS)_2$

Paul A. Mansky* and P.M. Chaikin
Department of Physics, Princeton University, Princeton, New Jersey 08544

R.C. Haddon
AT&T Bell Laboratories, Murray Hill, New Jersey 07974

(Received 16 May 1994)

We present evidence for and study the properties of coreless Josephson vortices (parallel to the superconducting layers) in the organic superconductor $(BEDT\text{-}TTF)_2Cu(NCS)_2$, using ac susceptibility measurements in the mixed state. We observe (1) extremely weak-pinning restoring forces for flux motion parallel to the layers, due to the absence of the vortex normal core; (2) single vortex (noncollective) pinning, due to weak interactions between Josephson vortices; (3) the "lock-in" of the vortices parallel to the layers when the dc field is applied at an arbitrary angle; and (4) highly nonlinear response to the ac field h in the lock-in state, above a threshold of $h \sim 0.5$ G. The behavior of tilted flux lines is dominated by the much stronger pinning and collective interactions of two-dimensional Abrikosov "pancake" vortices, and linear response is largely restored when the flux lines unlock from the layers. We measure the Josephson penetration depth to be $\lambda_\perp(T = 5\ \mathrm{K}) \sim 200\ \mu$m, yielding a penetration depth anisotropy of $\gamma = \lambda_\perp/\lambda_\parallel \sim 160 - 350$.

I. INTRODUCTION

Many superconductors of recent interest have layered crystal structures, and are believed to consist of two-dimensional superconducting planes coupled by Josephson tunneling. This has important effects on the structure and behavior of magnetic vortices. For flux lines making a large angle with the layers, the conventional picture of a vortex as a continuous, rigid flux tube must be replaced by a description of a flux line as a stack of two-dimensional "pancake" vortices in the individual layers[1–3] [Fig. 1 (top)]. These resemble a cross sectional slice of a conventional Abrikosov vortex. The field and supercurrent are distributed over a circular area with radius $\sim \lambda_\parallel$, the penetration depth associated with in-plane supercurrents; and the superconducting order parameter is suppressed within a normal core region of radius $\sim \xi_\parallel$, the in-plane coherence length. Pancake vortices in adjacent layers interact only weakly, via their magnetic fields and the tunneling currents, leading to greatly enhanced fluctuations of the vortex lines, and this can strongly affect the dc magnetization,[3,4] transport,[5] flux creep,[6] and other properties.

The interesting case of a magnetic field parallel or nearly parallel to the layers has been fairly well studied theoretically, but has received much less experimental attention. From the theoretical point of view, flux lines parallel to the layers are expected to differ from perpendicular vortices in two important ways. First, all length scales for the vortex lattice are highly anisotropic, being stretched out parallel to the layers.[7–9] Individual vortices have elliptical cross sections of area $\sim \lambda_\perp\lambda_\parallel$, where $\lambda_\perp = \gamma\lambda_\parallel$ is the Josephson penetration depth, associated with weak interlayer currents [Fig. 1 (bottom)]. The penetration depth anisotropy $\gamma > 1$ is a key parameter for characterizing a layered superconductor. The vortices are located on a distorted triangular lattice, with length scales $\sim \sqrt{\Phi_0/\gamma B}$ in the direction normal to the layers and $\sim \sqrt{\gamma\Phi_0/B}$ parallel to the layers,[9] and this has been confirmed by decoration experiments.[10]

Second, and more importantly, a vortex line parallel to the layers is believed not to have the usual normal core region.[11,12] This is often attributed to the fact that the interlayer spacing s exceeds the coherence length defined

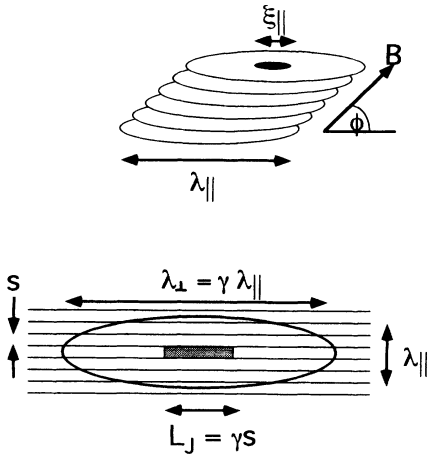

FIG. 1. Top: a tilted flux line consists of a stack of two-dimensional Abrikosov "pancake" vortices, each of which contains a normal core (dark area). The vortex makes an angle ϕ with the layers. Bottom: structure of a Josephson vortex, viewed along the field direction. The superconducting order parameter maintains its full value everywhere on the layers. The Josephson "core" (shaded area) is the region in which the tunneling current is comparable to the Josephson critical value J_0 and has width $L_J = \gamma s > \xi_\parallel$.

by $\xi_\perp = \xi_\parallel/\gamma$ below some crossover temperature, approximately given by $(T/T_c) = [1 - (\xi_\parallel(0)/\gamma s)^2]^{1/2}$, so that the normal core "fits between the layers." More precisely, the divergence of the current and magnetic field near the center of the vortex is cut off when the interlayer current becomes comparable to the Josephson critical current J_0. The in-plane currents remain small compared to the critical value $J_{c,0} \sim cH_c/\lambda_\parallel$, at which the kinetic energy density would become comparable to the condensation energy $H_c^2/8\pi$. (In a conventional Abrikosov vortex, the supercurrents become comparable to $J_{c,0}$ at $r \sim \xi$, and the order parameter goes to zero in order to avoid the divergence and minimize the total energy.) The order parameter can thus maintain its full value everywhere on the superconducting layers. The length scale over which the tunneling current is comparable to and limited by J_0 is the Josephson length $L_J = \gamma s > \xi_\parallel$, and L_J replaces $\xi_\parallel$ as the length scale for the Josephson vortex core in the direction parallel to the layers [Fig. 1 (bottom)]. Vortices parallel to the layers are in many ways similar to vortices parallel to a single Josephson junction[11] and are referred to as Josephson vortices.

The absence of the normal core for Josephson vortices has its most dramatic effects for flux lines tilted at very small angles $\phi \lesssim \tan^{-1}(1/\gamma)$ relative to the layers (see, for example, Refs. 14–19). In this angular regime, the vortex core consists of alternating two-dimensional (2D) normal cores and Josephson cores, linked together in a staircase fashion. One well-known experimental consequence of this is intrinsic pinning.[17,20] A large energy barrier opposes the motion of a Josephson vortex through the superconducting layers, leading to a suppression of the in-plane resistivity when the flux lines are nearly parallel. Closely related to this is the magnetic lock-in effect, in which the flux lines are trapped parallel to the layers even when the external field is applied at an angle. A transition to tilted vortices occurs when the applied perpendicular field component exceeds a threshold value. The lock-in effect was first observed experimentally in Bi-2212 by Zavaritskii and Zavaritskii,[23] through dc magnetization measurements. Anomalies in torque magnetization measurements have been observed in various high-T_c compounds at small tilt angles, and attributed to the effects of the layered structure.[21,22] Beyond this, there have been few experiments which directly probe the properties of Josephson vortices and relate them to the currently accepted theoretical models.

In a previous publication,[24] we presented evidence for the lock-in effect in the layered organic superconductor $(BEDT\text{-}TTF)_2Cu(NCS)_2$, hereafter referred to as "ET." The experimental probe was low frequency ac magnetic susceptibility, which allows the measurement of the vortex pinning force "spring constant" k_p, and the signature of the lock-in effect was a striking nonmonotonic behavior of the susceptibility (see below). The quantitative interpretation of the data focused almost exclusively on the angle and temperature dependence of the threshold field for the lock-in transition, and the details of the field, angle, and temperature dependence of the susceptibility were discussed only qualitatively. The data and analysis presented in this paper provide further strong evidence for the existence of Josephson vortices in ET, and show that the behavior of parallel flux lines is quite different than that of tilted flux lines in several respects. We list here a summary of our key findings:

Josephson penetration depth and anisotropy. We measure the penetration depth associated with interlayer currents to be $\lambda_\perp(5\text{ K}) \sim 200\ \mu$m, by studying the sample size dependence of the susceptibility in the Meissner state. Combined with $\lambda_\parallel \simeq 0.6$–$1.2\ \mu$m from other measurements, this gives an anisotropy of $\gamma \simeq 160$–330, in agreement with the result $\gamma \geq 200$ from torque magnetization measurements.[25]

Anisotropy of the microscopic pinning mechanism. The pinning force constant $k_p^\parallel$ for Josephson vortices moving parallel to the layers is extremely weak, due to the absence of the normal core; perpendicular vortices are pinned much more strongly, $k_p^\perp/k_p^\parallel \sim 500$. We relate the measured force constants to the appropriate energy and length scales for the vortex core: the condensation energy $H_c^2/8\pi$ and coherence length $\xi_\parallel$ for perpendicular vortices, and the Josephson coupling energy $\hbar J_0/2e$ and Josephson length $L_J = \gamma s$ for Josephson vortices. Based on our experimental results, we estimate the depinning critical currents for both types of vortices, and obtain fair agreement with the results of remnant magnetization measurements.[26]

Anisotropy of collective effects and the shear modulus. Despite the weakness of Josephson vortex pinning, $k_p^\parallel$ is independent of the vortex density (field strength), showing that the interactions between vortices are even weaker and do not affect the pinning. On the other hand, the pinning force decreases with field for perpendicular vortices, which we attribute to collective effects.[27] This is in agreement with calculations which show that the shear modulus of the vortex lattice is a factor of $\gamma^3 \simeq 10^7$ smaller in parallel fields as a result of the anisotropy.[9]

Magnetic lock-in effect. A magnetic field applied at an arbitrary angle with the layers initially penetrates the sample only in the form of weakly pinned Josephson vortices, leading to a rapid decay of ac screening. The vortices unlock from the layers when the perpendicular field component exceeds a threshold, and the screening recovers due to the onset of strong pinning of the pancake vortices.[24]

Scaling with normal field component. Well above the lock-in threshold, for angles larger than about 5°, the ac susceptibility is determined by the perpendicular field component, including the collective pinning effects. This shows that both the pinning and interactions of tilted flux lines are determined by the properties of the pancake vortices. We present a simple model which semiquantitatively reproduces the observed phenomenology over the whole range of fields and angles.

Nonlinearity in parallel fields. We observe highly nonlinear response (strong suppression of screening) to ac fields exceeding $h \sim 0.5$ G in the absence of perpendicular flux in the sample, i.e., in zero dc field or in the lock-in state. Linear behavior is largely restored when the flux lines unlock from the layers. While not yet fully understood, this effect further establishes that Josephson

vortices differ qualitatively from tilted vortices.

The experimental apparatus and techniques are described in reference Ref. 24. The insets to Figs. 6 and 10 show the configuration of the experiment and the shape of a typical crystal. The measurements described in this paper were made on a single sample, with dimensions $1.2 \times 0.8 \times 0.15$ mm^3, but all of the phenomena reported here have been observed in several samples (although measurements were made below 4.2 K on only one sample). The ac susceptibility was measured by a standard mutual inductance technique. The ac field **h** was parallel to the conducting layers and the longest sample dimension, and perpendicular to the dc field **H**. The sample could be rotated about the ac field axis with 0.0025° resolution, allowing the angle between **H** and the conducting planes to be varied while keeping **H** $\perp$ **h**. The ac field amplitude and frequency were 0.1 G and 2.5 kHz, except where otherwise noted.

An overview of the properties of the organic superconductor (BEDT-TTF)$_2$Cu(NCS)$_2$ is given in Ref. 28. The critical temperature $T_c \simeq 10$ K, and the interlayer repeat distance is $s \simeq 15$ Å. Other properties (upper and lower critical fields, coherence lengths, penetration depths) will be discussed at appropriate points in the text.

II. AC SUSCEPTIBILITY OF ANISOTROPIC SUPERCONDUCTORS

We begin with a brief discussion of the ac susceptibility of superconductors, including the effects of anisotropy and of elastic vortex motion in the mixed state. Dissipative vortex motion will be mentioned only briefly. Throughout this paper, we will use **H** and **h** to denote the applied (external) dc and ac fields, respectively, and **B** and **b** for the internal dc and ac magnetic fields. θ will denote the angle between **H** and the conducting layers, and ϕ is the angle between the layers and **B** [see, Fig. 13(a)].

The ac magnetic susceptibility of a superconductor, $\chi = M_{ac}/h$, is never exactly equal to $-1/4\pi$, the value associated with complete field exclusion (perfect Meissner effect). The applied field decays exponentially into the interior of the specimen, over the length scale of the penetration depth λ. If the field is applied parallel to an infinite slab of thickness L, it is easily shown (see Ref. 29, for example) that the susceptibility *per unit volume* is given by

$$-4\pi\chi = 1 - \frac{2\lambda}{L}\tanh\left(\frac{L}{2\lambda}\right), \tag{2.1}$$

which depends only on the ratio λ/L. The "screening strength" $-4\pi\chi$ is a conveniently normalized form of the susceptibility, with $-4\pi\chi = 1$ indicating complete exclusion of **h** ($\lambda \ll L$), and $-4\pi\chi = 0$ indicating complete ac field penetration ($\lambda \gg L$).

If the sample has a finite cross section $L_y \times L_z$ but the penetration depth is isotropic [Fig. 2(a)], Eq. (2.1) can still be used as long as the aspect ratio is large and field penetration across the smaller sample dimension (which we call L_z) dominates. For a superconductor with a large penetration depth anisotropy, however, the situation shown in Fig. 2(b) can occur, in which $\lambda_y/L_y \gtrsim \lambda_z/L_z$, and field penetration along the longer y direction can significantly contribute to or even dominate the permeability of the sample to the ac field. A more general equation for χ is therefore needed, which can be used for arbitrary values of λ_y/L_y and λ_z/L_z. We begin with the anisotropic London equation[7] for $b \parallel x$,

$$\lambda_y^2\frac{\partial^2 b}{\partial y^2} + \lambda_z^2\frac{\partial^2 b}{\partial z^2} - b = 0. \tag{2.2}$$

Following the derivation of Clem and Coffey[30] for the isotropic case ($\lambda_y = \lambda_z$), we obtain the equation

$$-4\pi\chi(\lambda_y, L_y, \lambda_z, L_z) = 1 - \frac{2\lambda_z}{L_z}\tanh\left(\frac{L_z}{2\lambda_z}\right) - \frac{16\lambda_y}{\pi^2 L_y}\sum_{n=0}^{\infty}\frac{\tanh(q_n L_y/2)}{(2n+1)^2(k_n^2\lambda_z^2+1)^{3/2}}, \tag{2.3}$$

with

$$k_n = \frac{2n+1}{L_z}\pi \qquad \text{and} \qquad q_n^2 = \frac{k_n^2\lambda_z^2+1}{\lambda_y^2}. \tag{2.4}$$

It is easily seen that Eq. (2.3) is a function only of λ_y/L_y and λ_z/L_z. We have checked both analytically and numerically that this equation gives physically reasonable results. If either $\lambda_i = 0$, Eq. (2.3) reduces to the form of Eq. (2.1), and if either or both $\lambda_i \to \infty$, $\chi = 0$. We have numerically verified that the results of Eq. (2.3) are symmetric under the interchange of the labels y and z. Keeping terms to $n = 50$ was found to be more than sufficient — summing to higher n did not lead to any

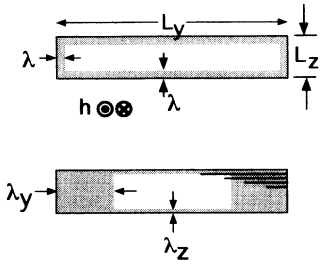

FIG. 2. Field penetration (shaded areas) in isotropic and anisotropic superconductors with rectangular cross sections. (a) For an isotropic superconductor, field penetration from the edges can be ignored if $L_y \gg L_z$. (b) This is not the case in an anisotropic superconductor if $\lambda_y/L_y \gg \lambda_z/L_z$.

observable changes in the results of calculations using Eq. (2.3).

The above discussion holds regardless of the mechanism of ac field penetration. In the Meissner state, λ_y will be the Josephson penetration depth $\lambda_\perp$, and λ_z the London penetration depth $\lambda_\parallel$. In the mixed state, the motion of vortices in response to the ac field provides another mechanism for ac field penetration. We will base our discussion of this on the simple model first proposed by Campbell[31] and later elaborated by other workers.[30,32–35] These are mean field models in the sense that the starting point is a single-vortex equation of motion. The parameters of the model are the pinning restoring force "spring constant" k_p and the viscosity η (see below), which are assumed to be the same for all vortices. Recent experimental work[36,37] has shown that this approach does not at all correctly describe the observed frequency dependence of the complex impedance, while models based on a scaling approach[38,39] work much better. Nonetheless, in the limit of low frequencies and linear response, the "mean field" approach seems to be an adequate framework for interpreting our results. Limited studies of the frequency dependence of the complex susceptibility in ET (Ref. 40) show a weak, roughly logarithmic frequency dependence, similar to that observed in Ref. 37 and Ref. 41. Order of magnitude changes in the frequency typically lead to only small changes in the susceptibility, which we take as justification for using the approximation of linear, elastic vortex motion.

We discuss the situation shown in Fig. 3, with the ac and dc fields perpendicular to each other; this corresponds to all of the experiments in the mixed state described in this paper. The dc field $\mathbf{H}$ establishes the vortex lattice and determines the average vortex density and orientation. The perturbing ac field $\mathbf{h}$ induces a screening current near the surface, and this exerts a force on the flux lines of $\mathbf{J} \times \mathbf{\Phi}_0/c$ per unit length, which

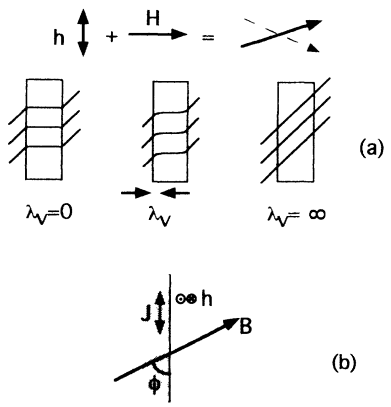

FIG. 3. (a) Relationship between ac field penetration and flux line pinning. The total external field $\mathbf{H} + \mathbf{h}$ executes a small amplitude tilting motion (top). Left: rigidly pinned flux lines: $\mathbf{B} = \mathbf{H}$ inside while $\mathbf{B} = \mathbf{H} + \mathbf{h}$ outside, and so $\chi_{ac} = -1/4\pi$. Right: if there are no forces opposing flux line motion, then $\mathbf{B} = \mathbf{H} + \mathbf{h}$ inside the sample and $\chi_{ac} = 0$. Center: in the general case, pinning forces lead to a vortex contribution λ_v to the ac penetration depth. (b) Geometry for discussion of angular dependence of λ_v.

causes them to tilt in the direction of the ac field. This force is balanced by pinning and viscous forces, according to the equation

$$\frac{1}{c}\mathbf{J} \times \mathbf{\Phi}_0 = k_p \mathbf{u} + \eta \dot{\mathbf{u}}, \tag{2.5}$$

where $\mathbf{u}$ is the displacement of the vortex from its equilibrium location. The pinning force constant k_p and viscosity η are per unit length of vortex. The tilting of the flux lines leads to enhanced penetration of the ac field. In the low frequency limit of this model, $\omega \ll \omega_0 = k_p/\eta$, the viscous forces can be ignored. The vortex displacements and the field and current distribution must be calculated self-consistently, and several workers[33,34] have shown that the resulting total penetration depth is

$$\lambda_{ac}^2 = \lambda^2 + \lambda_v^2 = \lambda^2 + \frac{B\Phi_0}{4\pi k_p}. \tag{2.6}$$

This is the equation which we will use throughout this paper [together with Eq. (2.1) or (2.3)] to determine the pinning force constant k_p from the susceptibility and penetration depth. The first term on the right hand side of Eq. (2.6) is the square of the London or Josephson penetration depth (depending on the geometry of the experiment), and the second term gives the square of the vortex motion contribution to the penetration depth λ_v^2.

This result applies to purely elastic and reversible vortex motion, and the complex susceptibility $\chi = \chi' + i\chi''$ is real ($\chi'' = 0$) and frequency independent. We do in fact observe a small but finite dissipation $\chi'' \neq 0$ (Fig. 6), and a weak, logarithmic frequency dependence.[40] However, the magnitude $|\tilde{\lambda}|$ of the complex penetration depth $\tilde{\lambda} = |\tilde{\lambda}|e^{i\delta}$ can be determined from χ' alone as long as χ'' is not too large. The phase angle δ can have any value between $\delta = 0$ (elastic dynamics) and $\delta = \pi/4$ (viscous dynamics, pure flux flow resistance). The complex impedance $\tilde{Z} \sim i\tilde{\lambda}^2$ is thus real (resistive) for $\delta = \pi/4$ and imaginary (reactive) for $\delta = 0$.[33,34] Figure 4 shows the real and imaginary parts of the susceptibility as a function of $|\tilde{\lambda}|$, for several values of δ. The calculations were made by expanding Eq. (2.1) into its real and imaginary

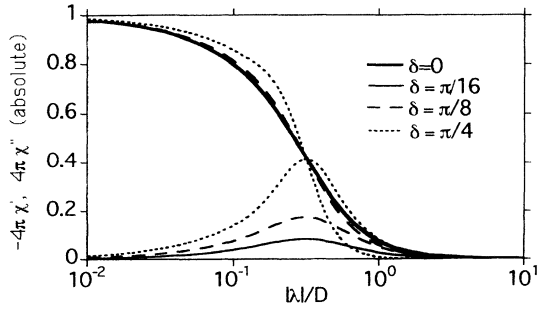

FIG. 4. Real and imaginary parts of the complex susceptibility $\chi(\tilde{\lambda})$ vs $|\tilde{\lambda}|$, with $\tilde{\lambda} = |\tilde{\lambda}|e^{i\delta}$, for $\delta = 0$ (purely reactive impedance), $\pi/16$, $\pi/8$, and $\pi/4$ (purely resistive impedance, $\tilde{\lambda}$ =classical skin depth). $\chi'(\tilde{\lambda})$ depends only weakly on δ for $\delta \leq \pi/8$.

parts.[29] It can be seen that for $\delta \lesssim \pi/8$ (corresponding to a small peak in χ''), χ' is determined to good accuracy by $|\tilde{\lambda}|$ only, as claimed above.

If the vortices make an angle ϕ with the surface but are still perpendicular to the ac field [Fig. 3(b)], Eq. (2.6) is replaced by[32,34]

$$\lambda_{ac}^2 = \lambda^2 + \frac{B\Phi_0}{4\pi k_p(\phi)} \sin^2\phi, \tag{2.7}$$

where we have allowed for a possible angular dependence of the pinning force constant k_p. One factor of $\sin\phi$ arises from the angular dependence of the Lorentz force between the vortex and the surface currents, $\mathbf{F} = \mathbf{J} \times \mathbf{\Phi}_0/c$, and the other is essentially due to the fact that the ac field is most effectively transmitted along the direction of the flux lines, which are parallel to B. λ_v is zero when the vortices are parallel to the surface ac screening currents.

III. MEASUREMENT OF THE JOSEPHSON PENETRATION DEPTH

The in-plane penetration depth $\lambda_\parallel$ of (BEDT-TTF)$_2$Cu(NCS)$_2$ has been measured by muon spin precession,[42] reversible dc magnetization,[43] and microwave cavity perturbation,[44] which give values of $\lambda_\parallel(0)$ ranging from 0.65 μm to 1.2 μm. The anisotropy γ can then be determined in a number of ways. The upper critical fields at $T = 0$, determined from the transition in the in-plane resistance,[45] are $H_{c2}^{\parallel}(0) \simeq 20$ T and $H_{c2}^{\perp} \simeq 5$ T, yielding $\gamma \simeq 4$. A similar anisotropy was obtained from specific heat measurements[46] of the critical fields close to T_c. (A larger anisotropy, $\gamma \sim 20$, is obtained from the resistive phase boundaries near T_c, due to the positive curvature of the resistive phase boundary.[45]) However, γ is related to the critical field anisotropy in this way only if $H_{c2}^{\parallel}$ is determined by orbital effects, e.g., the overlap of the normal cores. The critical field measurements give $\xi_\parallel(0) \simeq 80$ Å and $\xi_\perp = \xi_\parallel/\gamma \simeq 20$ Å $\sim s$, suggesting that ET is at least close to the limit of weakly coupled layers and that some other mechanism might determine $H_{c2}^{\parallel}$. We note that $H_{c2}^{\parallel}(0)$ is fairly close to the Pauli pair-breaking limit of (18.4 kG/K)$\times T_c$.

A much larger anisotropy, $\gamma \geq 200$, was obtained from reversible torque magnetization experiments,[25] implying that $\lambda_\perp \simeq 130$–240 μm. Kanoda *et al.*[47] measured $\lambda_\perp(T)$ of ET directly, using calibrated low frequency ac susceptibility measurements in the Meissner state, and found a macroscopic value of $\lambda_\perp(0) \sim 1$ mm. Although this result was controversial, it is at least consistent with the lower limit from the torque measurements. dc susceptibility experiments had previously provided evidence for macroscopically large Josephson penetration depths in the organic superconductor (TMTSF)$_2$ClO$_4$ (Ref. 48) and in the intercalation compound TaS$_2$(py)$_{1/2}$.[49]

We have used the method of Kanoda *et al.*[47] for measuring $\lambda_\perp$. We focus on the size of the penetration depth at one temperature, not the details of the temperature dependence, and have taken data only down to $T \sim 4.5$ K$\sim T_c/2$. The real part of the susceptibility $\chi'(T)$ was measured for five ET samples of various sizes, in the geometry shown in the inset to Fig. 5(b). The apparatus was calibrated using reference samples of three conventional superconductors, slabs of Nb, Pb, and Ta with dimensions similar to the ET crystals. The reference samples gave sharp transitions in χ' at the correct T_c's, and the ratio of the step in the coil output to the sample volume was the same for all three samples, to about 5% accuracy. The reference samples were thus assumed to have a susceptibility of $-1/4\pi$ per unit volume.

Measurements were made on five ET crystals. The absolute values of the screening strength per unit volume $-4\pi\chi'(T)$ for three of the samples are plotted in Fig. 5(a). Recall that $-4\pi\chi' = 1$ indicates a perfect Meissner effect. The transitions are broad, the screening does not saturate down to $T = 4.5$ K$\sim T_c/2$, and the screening *per unit volume* is weaker for smaller samples. The same data are shown again in Fig. 5(b), normalized to approximately coincide at $T = 5$ K. It can be seen that the transition is sharper for larger samples. All of these features are qualitatively consistent with the behavior expected if one of

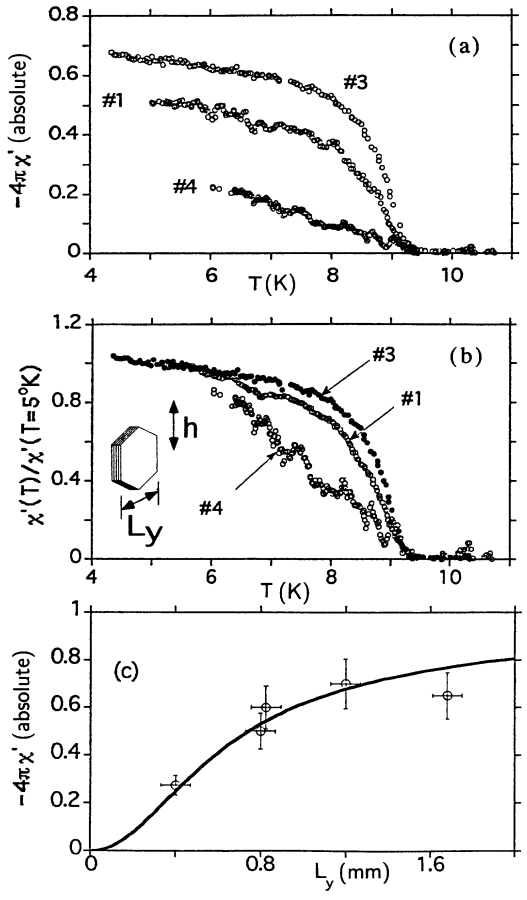

FIG. 5. (a) Absolute value of the screening strength $-4\pi\chi'$ for three samples with different lengths L_y. (b) Same data as in (a), normalized to coincide at $T = 5$ K. (c) $-4\pi\chi'$ (5 K) vs L_y for all five measurements. The fit is described in the text, and gives $\lambda_\perp$ (5 K)=200 μm.

the penetration depths is comparable to the appropriate sample dimension. Because the in-plane penetration depth $\lambda_{\|}(0) \sim 1$ μm is much smaller than the typical sample thickness $L_z \sim 100$ μm, field penetration normal to the layers cannot be responsible for this behavior. We therefore attribute it to a macroscopically large penetration depth $\lambda_\perp$ associated with interlayer currents, and assume that the situation is as shown in Fig. 2(b).

The value of $\lambda_\perp$ at $T = 5$ K was obtained by fitting $\chi'(T = 5\ \text{K})$ from all five samples to Eq. (2.1), with the penetration depth $\lambda_\perp(T = 5\ \text{K})$ as the only fitting parameter [Fig. 5(c)]. The quality of the fit is fairly good, showing that the susceptibilities of all of the samples can be explained by the same value of the penetration depth $\lambda_\perp$, and the result is $\lambda_\perp(5\ \text{K}) \simeq 195 \pm 20$ μm. The penetration depth $\lambda_\perp$ and Josephson critical current J_0 are related by $J_0 = c\Phi_0/8\pi^2 s\lambda_\perp^2$, which gives $J_0 \simeq 400$ A/cm^2. Given the range of reported values 0.55 μm $\leq \lambda_{\|} \leq 1.2$ μm, using $\lambda_\perp(0) \sim 200$ μm gives $160 \leq \gamma \leq 350$ for the anisotropy. This is consistent with the torque result,[25] $\gamma \geq 200$. Tokumoto *et al.*[50] observed similar behavior of the dc susceptibility with a weak field parallel to the layers, and we obtain $\lambda_\perp(T = 5\ \text{K}) \simeq 200$ μm from an analysis of their data. (The two largest dimensions of their sample were 1.2 and 0.7 mm. We use $L_y = 1$ mm since the orientation of the field is not specified in Ref. 50.) We can only attribute the discrepency between our result and the value of ~ 1 mm of Kanoda *et al.*[47] to a difference in sample quality. Cracks in a sample would reduce the effective sample size, leading to enhanced ac field penetration and an overestimate of $\lambda_\perp$

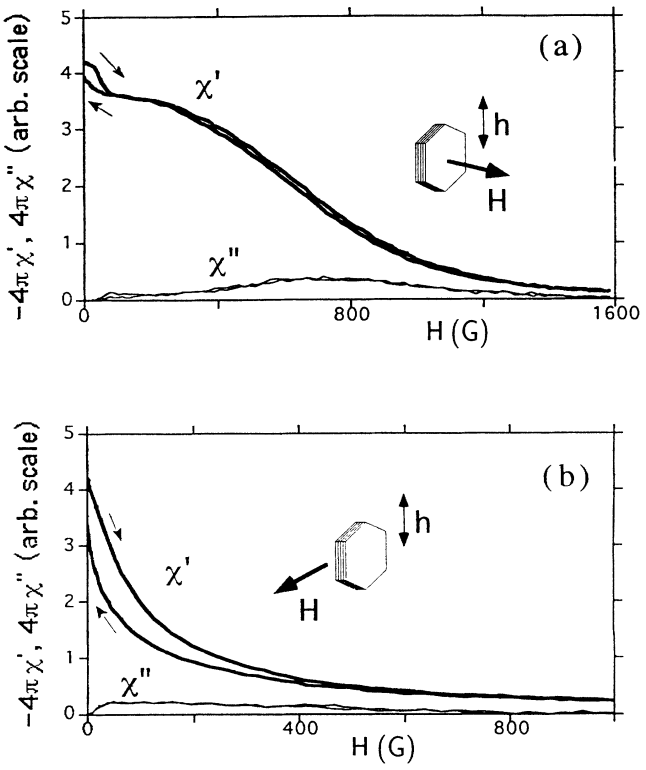

FIG. 6. Real and imaginary parts of the complex susceptibility at $T = 4.2$ K, with the dc magnetic field applied (a) normal to the layers, and (b) parallel to the layers.

IV. PINNING MECHANISM ANISOTROPY

Application of a dc magnetic field **H** either parallel or perpendicular to the conducting layers (and perpendicular to the ac field **h**) causes a monotonic decrease of the screening strength $-4\pi\chi'$, as shown for $T = 4.2$ K in Figs. 6(a) and 6(b), but the behavior of $\chi(H)$ in these two orientations differs in several ways: (1) The screening $-4\pi\chi'(H)$ decreases much more rapidly for **H** parallel to the layers. This is the *opposite* of the anisotropy in the resistively determined critical fields $H_{c2}^{\perp} \sim 2$ T and $H_{c2}^{\|} \sim 17$ T. The midpoint of the "transition" in $\chi'(H)$ for **H** parallel to the layers occurs at $H \sim 100$ G, *a factor of* $\sim 10^3$ *lower* than the parallel field resistive transition at ~ 17 T.[45] (2) The form of $\chi'(H)$ is qualitatively different for the two orienations, with a roughly Gaussian shape for perpendicular **H**, and positive curvature throughout, and a long tail at high fields for parallel **H**. (3) The peak in the imaginary part $\chi''(H)$ is larger for perpendicular **H**. (4) The field above which $\chi'(H)$ is *reversible* (for H increasing and decreasing) is much lower for the perpendicular orientation. In this section, we present data in both orientations over the temperature range 2.4–9 K, and focus on the interpretation of features (1) and (2) in terms of the anisotropy of the microscopic pinning mechanism and of the shear modulus for parallel and perpendicular vortices. The differences in dissipation and reversibility will not be discussed in detail.

In Fig. 7(a) we show $-4\pi\chi'(H)$ for several temperatures between 2.4 K and T_c, with **H** parallel to the layers. The susceptibility for $H = 0$ is determined by $\lambda_\perp(T)/L_y$, where $\lambda_\perp(T)$ is the Josephson penetration depth (as in Fig. 5), while the decay of χ' with increasing field is due to vortex motion (Sec. II). The vortices are parallel to the layers, and are driven by interlayer currents flowing at the edges of the sample. The resulting tilting motion parallel to the layers leads to enhanced ac field penetration along the y direction only, not along z [inset to Fig. 7(a)]. With reference to Fig. 2, $\lambda_z = \lambda_{\|}(T)$ is independent of field and $\lambda_z/L_z \ll 1$. We may therefore entirely neglect ac field penetration from the faces, and use the simple one-dimensional equation (2.1) for $\chi(\lambda_y/L_y)$. The solid lines are fits to Eq. (2.1) with the field- and temperature-dependent penetration depth given by Eq. (2.6),

$$\lambda_y^2 = \lambda_\perp^2(T) + \frac{B\Phi_0}{4\pi k_p^{\|}(T)}, \tag{4.1}$$

with the pinning force constant $k_p^{\|}$ a *constant* for each fit. The fit is very good at all temperatures, and the values of $k_p^{\|}$ extracted from these data sets (and others not shown) are shown in the inset to Fig. 7(a). The typical value of the restoring force constant is $k_p^{\|} \sim 10^{-3}$ dyn/cm^2.

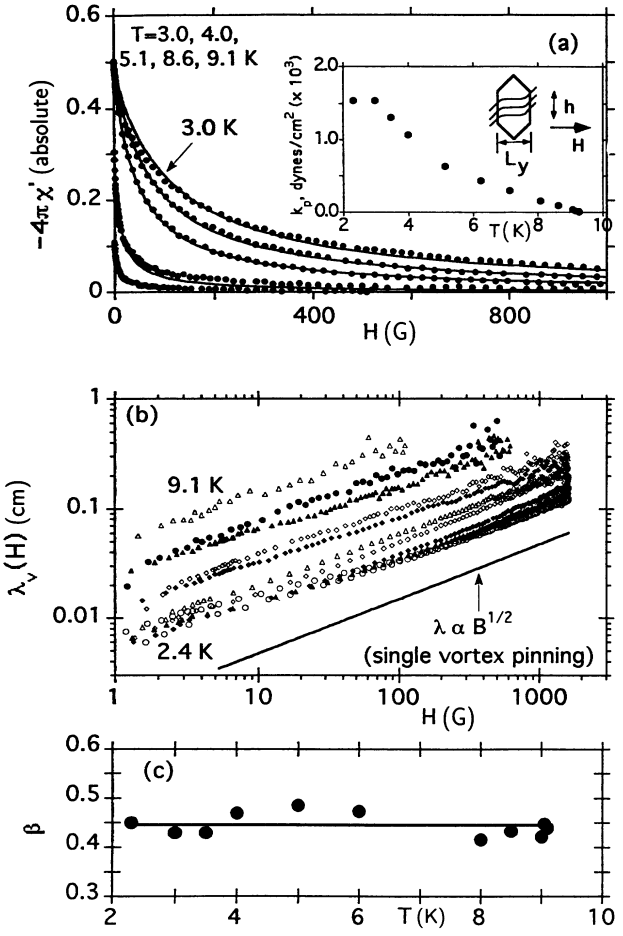

FIG. 7. (a) $-4\pi\chi'(H)$ with **H** parallel to the layers, at various temperatures (points). Fits are described in text. Inset: values of $k_p^{\parallel}(T)$ from fits. Vortices allow enhanced ac field penetration along y, and χ' is determined by λ_y/L_y. (b) Vortex motion contribution to the ac penetration depth vs field, extracted from susceptibility data as described in text. Solid line shows $\lambda_v \sim \sqrt{B}$ behavior expected for single-vortex pinning. Fits to a power law field dependence, $\lambda_v \sim H^{\beta}$, give an average power $\beta \simeq 0.45$ (c).

This is extraordinarily small compared to typical values for the high-T_c superconductor YBCO: $k_p(T=0) \sim 10^6$ dyn/cm^2 for single-crystal YBCO,[51] and $k_p \sim 1$ dyn/cm^2 for vortices trapped *between grains* in granular YBCO.[52] We discuss the relationship of $k_p^{\parallel}$ to the microscopic pinning mechanism in Sec. IV B.

We obtain the field-dependent part of the penetration depth from the data by numerically inverting Eq. (2.1) to obtain $\lambda_y(H,T)$, using $L = L_y = 0.8$ mm. (We neglect χ'' in determining the penetration depth, as discussed in Sec. II.) This was done using an algorithm which chooses successively better values of λ_y until finding one which gives the correct value of χ' to an accuracy of 10^{-3}. From Eq. (4.1), the vortex contribution $\lambda_v(H)$ is then $\lambda_v(H) = \sqrt{\lambda_y^2(H,T) - \lambda_\perp^2(T)}$. $\lambda_v(H)$ is plotted on a log-log scale in Fig. 7(b), and is well described by a power law $\lambda_v(H) \sim H^{\beta}$ at all temperatures. The values of β obtained from power law fits are shown in Fig. 7(c), and have an average value of 0.45. This is consistent with the good quality of the fits shown in Fig. 7(a), for which β is fixed at 0.5. The observation that $\lambda_v \sim \sqrt{H}$ and $k_p^{\parallel} \simeq$const for parallel **H** implies that *the pinning force for each vortex is independent of the total vortex density*, and is therefore unaffected by interactions between vortices. This is the case of "single-vortex pinning," in the terminology of collective pinning theory.[27] We will discuss the self-consistency of this finding in Sec. IV A.

Figure 8(a) shows a similar data set for the perpendicular field orientation. Again, the susceptibility in zero field is determined by ac field penetration in the y direction, due to the large Josephson penetration depth $\lambda_\perp(T) = \lambda_y$. The vortices are now normal to the large surfaces of the crystal, and interact with in-plane surface currents; so the resulting tilting motion leads to additional ac field penetration in the z direction. The full two-dimensional susceptibility formula (2.3) must there-

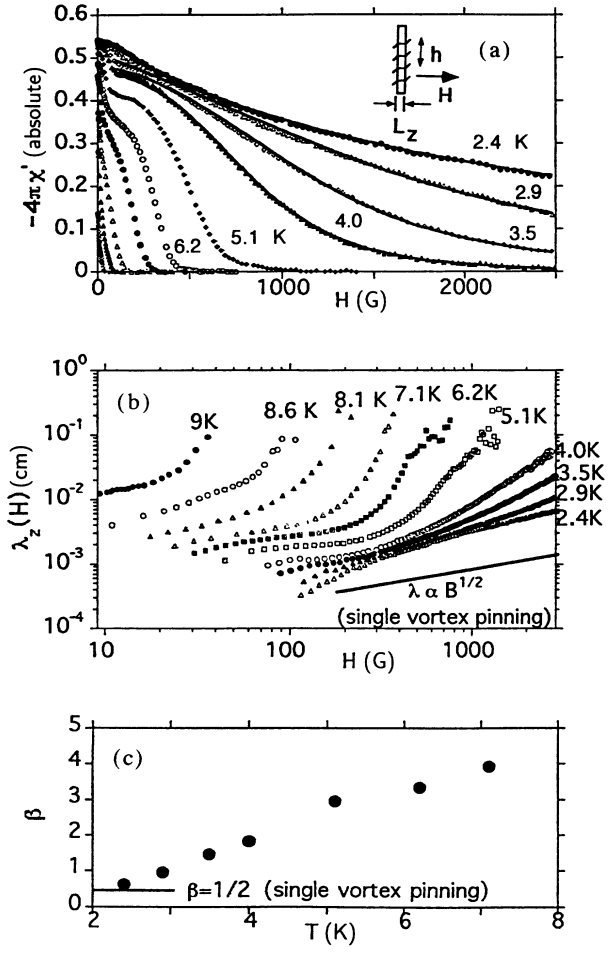

FIG. 8. (a) $-4\pi\chi'(H)$ with **H** perpendicular to the layers, at various temperatures. Solid lines through the data are fits to power law field dependence of λ_v; see text. (b) λ_v vs H, extracted from the data of figure (a) as described in text. λ_v increases faster than $\sqrt{H}$, indicating collective pinning effects. (c) Temperature dependence of power β, obtained by fitting high-field data in (b) to a power law, $\lambda_v(H) \sim H^{\beta}$.

fore be used in analyzing the data. The form of $\chi'(H)$ varies *qualitatively* as the temperature is varied, and resembles the parallel field data only at the lowest temperature studied, 2.4 K. At this temperature, the susceptibility can be fit using Eq. 2.3, with $\lambda_y = \lambda_\perp(T)$ =const and $\lambda_z(B) = B\phi_0/4\pi k_p^\perp$, resulting in $k_p^\perp(2.4\text{ K}) \simeq 0.7$ dyn/cm^2 and $k_p^\perp/k_p^\parallel \simeq 500$ at this temperature. To better understand how this anisotropy is implied by the data, recall that the decay of the susceptibility is determined by λ_y/L_y when the vortices are parallel to the layers, and by λ_z/L_z when they are perpendicular. Thus for a fixed value of the screening strength (e.g., $-4\pi\chi' = 0.3$, occurring at fields $B_\parallel^* \simeq 80$ G and $B_\perp^* \simeq 1500$ G), it must be true that the vortex contributions to λ_z/L_z and λ_y/L_y are equal, or

$$\frac{B_\parallel^*}{L_y^2 k_p^\parallel} = \frac{B_\perp^*}{L_z^2 k_p^\perp}. \tag{4.2}$$

The pinning anisotropy is thus determined by both the ratio of field scales for the decay of screening, and the *square* of the sample aspect ratio: $k_p^\perp/k_p^\parallel \simeq (B_\perp^*/B_\parallel^*)(L_y/L_z)^2 = (1500/80)(0.8/0.15)^2 \simeq 500$. We will discuss the relationship of the measured $k_p^\perp$ to the microscopic pinning mechanism in Sec. IV B.

At intermediate temperatures (about 3.5 – 7.1 K), a different type of behavior occurs in perpendicular fields, with a "bump" at low fields and a roughly Gaussian or bell shape above this. Above 7.1 K, $\chi'(H)$ again has positive curvature everywhere (as at the lowest temperature), but now goes to zero more abruptly, without the gradual tail which occurs at other temperatures. The field at which $\chi' \to 0$ is much smaller than the resistively determined critical field $H_{c2}^\perp(T)$ at all temperatures. $\chi'(H)$ is reversible with increasing and decreasing dc field above the low-field bump and irreversible in the low-field region [Fig. 6(a)]. The magnitude of the reversibility field is about double that of reported values of the lower critical field $H_{c1}^\perp$, as determined by dc magnetization experiments,[26,50] and has similar temperature dependence (with positive curvature). We focus on the behavior at high fields, and do not discuss the low-field region further.

With $\lambda_y = \lambda_\perp(T)$ determined from $\chi'(H = 0)$, $\lambda_v = \lambda_z(H,T)$ can be determined from the data by numerically inverting Eq. (2.3), using the same type of algorithm used in analyzing the parallel field data. We again ignore the imaginary part χ''. The results of this procedure are shown in Fig. 8(b), on a log-log plot. The data for $T \leq 7.1$ K appear to be approaching power law field dependence $\lambda_v \sim H^\beta$ at high fields, but with a temperature-dependent power β. The asymptotic value of β is plotted against the temperature in Fig. 8(c). $\lambda_v(H)$ in the reversible region was fit to the form $\lambda_v(B) = a + bH^\beta$ for $T \leq 4.2$ K , and the parameters obtained from the fits were used to calculate the solid lines in Fig. 8(a). Note that the largest values of λ_z correspond to the smallest values of $-4\pi\chi'$, and the sensitivity is greatest when $\lambda_z \sim L_z$. The sensitivity of the measurement is lost when λ_z becomes much larger than $L_z = .015$ cm, and this is why data are not available for higher fields at higher temperatures.

We cannot at present quantitatively account for observed field and temperature dependence, but can make some general statements. One expects that $\lambda_v \sim \sqrt{B}$ only if k_p is field independent, and this implies single-vortex pinning. Whether or not $\lambda_z(H)$ is actually well described by a power law, it is clear from Fig. 8 that the penetration depth generally increases *faster* than $\sqrt{B}$, and this indicates that the average pinning force constant k_p becomes weaker as the field is increased. A likely mechanism for the softening of the pinning strength at higher temperatures is collective pinning, as first proposed by Larkin and Ovchinnikov.[27] Collective pinning results from the competition between repulsive intervortex interactions (elasticity), which favor long range periodic order, and pinning by a random potential with no long range order. If elasticity is dominant, the flux lines are essentially randomly distributed with respect to the pinning potential minima. The effective restoring force constant for each vortex will then vary in sign, depending on whether the curvature of the pinning potential is positive or negative at the equilibrium location of the flux line [e.g., for a pinning potential of the form shown in Fig. 9(c)]. This leads to a reduction of the *average* pinning force constant when k_p is averaged over the field-dependent correlation volume[27] V_c. Because the elastic constants increase with field at low fields, the correlation volume grows and the average pinning force constant becomes weaker as the field is increased. Collective pinning is usually used to explain the decrease of the critical current with increasing vortex density.

The data therefore suggest that at the lowest studied temperature of 2.4 K (and presumably below this as well), perpendicular flux lines are pinned individually, while the pinning becomes collective at higher temperatures, presumably due to the weakening of the pinning potential by thermal fluctuations. The field dependence of χ' was similar in all samples studied for $T > 4.2$ K, but only one sample was studied down to $T = 2.4$ K. Thus our claim of a temperature-driven *transition* from single-vortex to collective pinning is based on one sample only, but the claims of collective pinning for $T \geq 4.2$ K and single-vortex pinning in parallel fields at all temperatures are based on results from several samples. A temperature-driven transition from individual to collective pinning was observed in YBCO single crystals for $H \parallel c$, by Krusin-Elbaum *et al.*[53] They found that the critical current J_c [deduced from the dc magnetization $M(H)$ using the Bean model] was field independent for $T < 45$ K , and decreased as $J_c \sim 1/H^3$ at high temperatures.

We now consider in more detail whether the above results are self-consistent, and consistent with theoretical ideas about collective pinning and microscopic pinning mechanisms.

A. Collective effects: Anisotropy of the shear modulus

The observation of individual pinning of Josephson vortices and collective pinning of perpendicular vortices

may seem contradictory at first. Single-vortex pinning occurs when pinning forces exceed elastic forces, but Josephson vortices are 500 times more *weakly* pinned than perpendicular vortices, according to the results of our experiments. However, the anisotropy of the elastic constants must also be taken into account.[9,54] To determine whether our findings are self-consistent, we can make a crude estimate of the effective restoring force due to the vortex elasticity in both orientations, and compare this to the measured values of k_p. We do this by considering a shear wave, with displacement amplitude u and wave vector $\mathbf{q} \perp \mathbf{u}$. The free energy per vortex and per unit length is[55] (in cgs units)

$$f = \left[\frac{\Phi_0}{B} C_{66} q^2\right] u^2. \tag{4.3}$$

We take the coefficient of u^2 to be an effective restoring force constant due to interactions, and wish to compare this to k_p.

We first consider the case of flux lines perpendicular to the layers. Since we are interested in independent displacements of neighboring vortices, we take $q \sim 1/a = \sqrt{B/\Phi_0}$, and 4.3 simplifies to $C_{66}u^2$. The shear modulus for perpendicular flux lines (for $H_{c1} \ll H \ll H_{c2}$) is the same as for an isotropic superconductor[55] with penetration depth $\lambda_\parallel$, $C_{66}^\perp = B\Phi_0/(8\pi\lambda_\parallel)^2$. Using $\lambda_\parallel \simeq 1$ μm, we get $C_{66} \simeq 0.03\ B$ with the magnetic field B in gauss. (C_{66} and k_p both have units of ergs/cm^3 =dyn/cm^2). The pinning constant $k_p^\perp \simeq 0.7$ dyn/cm^2, and the elastic energy exceeds the pinning energy for $B \gtrsim 30$ G. Thus, far from it being surprising that collective effects are observed, it is puzzling that single-vortex pinning is observed at all in kG fields, even at low temperatures.

A temperature-driven transition from single-vortex to collective pinning was predicted by Koshelev and Vinokur[56] and by Feigel'man, Geshkenbein, and Larkin (AGL),[57] who predicted that that single-vortex pinning should occur for sufficiently small B and T. However, the crossover temperatures predicted by these models for ET are on the order of $T = 5$ mK. This small value results from the use of $k_p^\perp(T = 2.4\ \text{K}) \simeq 1$ dyn/cm^2 in calculating the parameters which go into the the models: the depinning critical current $j_c^\perp \simeq k_p^\perp \xi_\parallel(0)c/\Phi_0 \sim 25$ A/cm^2 (see next section) for the calculation in Ref. 56, and the pinning energy per 2D vortex $U_p \simeq k_p^\perp \xi_\parallel^2 s \simeq 1$ mK for the calculation in Ref. 57. The reason for this discrepancy is not understood. The observed crossover temperature for YBCO in Ref. 53, ~ 45 K. agreed fairly well with estimates from these models.

For vortices parallel to the layers, there is both a "hard" and an "easy" shear modulus, corresponding to shear parallel (C_{66}^e) or perpendicular (C_{66}^h) to the layers. Ignoring the discreteness of the layers, i.e., in the anisotropic Ginzburg-Landau model, Kogan and Campbell[9] obtained $C_{66}^{(e)} = C_{66}^\perp/\gamma^3$ and $C_{66}^h \simeq \gamma C_{66}^\perp$. We have simplified Kogan and Campbell's equation (9) using the identities for the reduced effective masses in their model, $m_1 = 1/\gamma^{2/3}$ and $m_3 = \gamma^{4/3}$. Since the layered structure only affects the structure of the core, the AGL result for C_{66}^e should also apply to layered materials. The easy shear modulus for Josephson vortices is thus a factor of $\gamma^3 \sim 10^7$ *weaker* than the shear modulus for perpendicular vortices, and the anisotropy of the shear modulus is much larger than the pinning constant anisotropy, $k_p^\perp/k_p^\parallel \sim 500$.

Shear parallel to the layers should dominate the distortion of the lattice. We therefore take u parallel to the layers and q perpendicular to the layers, and set $q \simeq \sqrt{\gamma B/\Phi_0}$ to account for the anisotropy of the lattice structure. Using this in Eq. (4.3), the prefactor of u^2 in the expression for f is $\gamma C_{66}^{(e)} \simeq 8 \times 10^{-7} B$ dyn/cm^2, with B in gauss. We again identify this as an effective force constant due to vortex interactions in the presence of shear. This does not become comparable to the measured pinning force constant $k_p^\parallel \sim 10^{-3}$ dyn/cm^2 until $B \sim 1$ kG. Furthermore, the calculation of Kogan and Campbell[9] was in the local limit, $q = 0$, while vortex lattice elastic moduli can be highly dispersive. A numerical calculation by Sudbo and Brandt[54] showed that a very significant further suppression of $C_{66}^{(e)}$ occurs for q near the Brillouin zone boundary. It is thus not at all unreasonable for the extremely weak measured pinning forces to exceed the even weaker elastic forces which occur in parallel fields.

B. Microscopic pinning mechanisms and critical current: Condensation energy and coupling energy

We now relate the measured pinning force constants to models of the microscopic pinning mechanisms for Abrikosov and Josephson vortices, and to values of the depinning critical current obtained from remnant magnetization experiments.[26]

The basic principle of normal core pinning by a defect is shown in Fig. 9(a). It is energetically favorable for a defect which suppresses superconductivity to be situated in the center of a vortex normal core; separating the vortex from the defect causes further suppression of superconductivity by the defect and an increase in the energy. An upper limit on the pinning energy per unit length of a perpendicular vortex line is given by the total condensation energy in the core, which is approximately $U \sim (H_c^2/8\pi)\xi_\parallel^2$. The range of the pinning potential is $r_p \sim \xi_\parallel$, and so an upper limit on the linear restoring force per unit length is $k_p \sim U/r_p^2 \sim H_c^2/8\pi$. For ET, $H_c(0) \sim 500$ G (Ref. 47) and $H_c^2/8\pi \simeq 10^4$ dyn/cm^2. The measured pinning constant for perpendicular vortices is about 1 dyn/cm^2 at 2.4 K, and so the observed pinning force constant is a factor of $p = 10^4$ times weaker than the maximum core pinning value. The coherence length $\xi_\parallel(0) \sim 80$ Å, and the weakness of the measured pinning constant thus seems to indicate that pinning is due to very weak, atomic scale ($d \ll \xi_\parallel$) defects. In single-crystal YBCO, strong pinning is observed[51] ($p \sim 1$), due in part to the fact that the coherence length $\xi_{ab}(0) \sim 10$ Å is similar in size to the atomic scale defects. Values of $p \sim 10^{-3}$ are typical for conventional superconductors.[13]

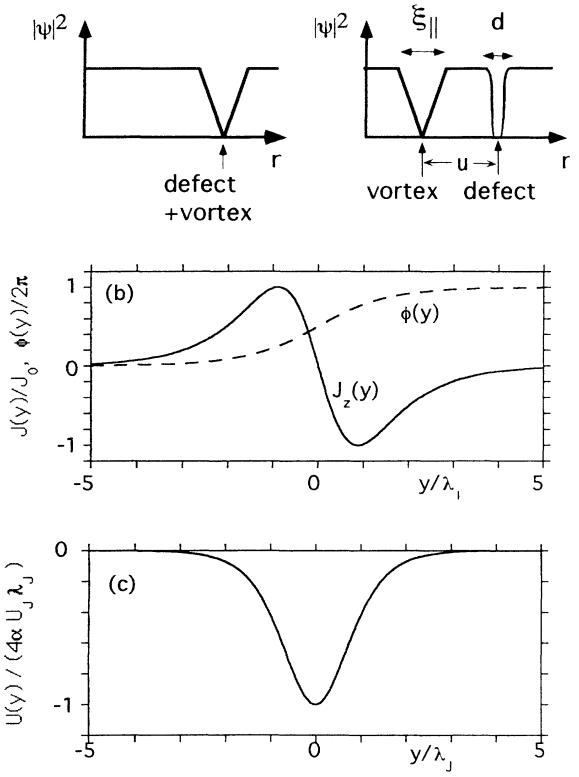

FIG. 9. (a) Schematic of core pinning mechanism. Separating the vortex and defect by a distance $u > \xi$ raises the energy per unit length by at most $\sim (H_c^2/8\pi)\xi^2$. (b) Spatial variation of the phase and tunneling current of a fluxon in a single Josephson junction. λ_J is the only length scale. In a layered superconductor, $J \sim J_0$ for $|y| \sim L_J \equiv \gamma s$, while for large $|y|$ the current decays as $\exp(\pm y/\lambda_\perp)$. (c) Pinning potential for a perturbation $\delta J_0/J_0 = \alpha\delta(y)$, for a fluxon in a single junction. The depth of the well is $\sim 4\alpha U_J \lambda_J$ and the range of the potential is $\sim \lambda_J$.

In a similar spirit, we may estimate an upper limit for the pinning constant of a Josephson vortex in a layered material, for motion parallel to the layers. We first consider a simpler and previously studied case, pinning of a fluxon in a single Josephson junction.[58,59] The coupling energy E_c (per unit area) between the superconductors depends on the gauge-invariant phase difference $\Delta\varphi$ between them, and is given by

$$E_c = U_J(1 - \cos\Delta\varphi), \tag{4.4}$$

where $U_J = \hbar J_0/2e$ gives the scale for the coupling energy, and the phase difference is related to the Josephson current by $J = J_0 \sin\Delta\varphi$. The spatial variation of the phase for a fluxon is given by the phase soliton solution, $\Delta\varphi_0(y) = 4\tan^{-1}[\exp(y/\lambda_J)]$ [Fig. 9(b)], and the Josephson penetration depth λ_J gives the scale for both the decay of the tunneling current at large y and the size of the "core" region near $y = 0$, in which the tunneling current is comparable to and limited by J_0.

Translational symmetry in the y direction is broken by random variations of the coupling J_0, e.g., of the form $J_0(y) = [1 + f(y)]J_0$. Regions with $f < 0$ correspond to weaker than average coupling, and act as pinning sites. If $|f| \ll 1$, the additional energy due to f can be calculated perturbatively:

$$\delta U = -U_J \int_{-\infty}^{+\infty} f(y)\cos\Delta\varphi_0 dy. \tag{4.5}$$

One then expects the total pinning energy to be on the order of $(U_J\lambda_J)\langle f^2\rangle^{1/2}$, per unit length. The upper limit for the pinning energy is thus $\epsilon_J = U_J\lambda_J$, and that for the restoring force constant is $\epsilon_J/\lambda_J^2 = U_J/\lambda_J$. This is in agreement with more detailed calculations. For a line defect, with $f(y) = \alpha\delta(y)$ and $\alpha \ll 1$, the pinning energy is[58] $4\alpha\epsilon_J$. Figure 9(c) shows the pinning potential for this case. If $f(y)$ is random, with correlation length l, then the scale for the pinning energy is[59] $\epsilon_J[(l/\lambda_J)\langle f^2\rangle]^{1/2}$.

The structure of a Josephson vortex in a layered material differs from that of a fluxon in that there are *two* length scales parallel to the layers:[11] the penetration depth $\lambda_\perp$, which governs the exponential decay of the field and current at large distances, and the Josephson length $L_J = \gamma s$, which governs the behavior of the core region in which $J \sim J_0$. The core region should account for most of the pinning energy, due to the large currents and small length scale. Considering only the contribution of the central junction ($z = ns = 0$) to the pinning,[60] the upper limit on the pinning force constant is

$$k_p^{\parallel} \lesssim \frac{U_J}{L_J} = \frac{1}{\gamma s}\frac{\hbar J_0}{2e} = \frac{1}{16\pi^3\gamma}\left(\frac{\Phi_0}{s\lambda_\perp}\right)^2, \tag{4.6}$$

where we have used $\Phi_0 = hc/2e$ and $J_0 = c\Phi_0/8\pi^2 s\lambda_\perp^2$. Using $\gamma \sim 250$, $s = 15$ Å, and $\lambda_\perp \sim 200$ μm gives $k_p^{\parallel} \lesssim 3\times10^{-2}$ dyn/cm^2, and this is only a factor of ~ 30 higher than the typical values ($\sim 10^{-3}$ dyn/cm^2) measured in ET at low temperatures.

The pinning force constant can be approximately related to the depinning critical current J_c if one assumes that the force is linear over most of the range r_p of the potential. The critical current is then defined by the force equation for a single vortex, $F_{\max} = J_c\Phi_0/c \simeq k_p r_p$, which gives

$$J_c \simeq k_p r_p \frac{c}{\Phi_0}. \tag{4.7}$$

For perpendicular vortices, with $k_p^{\perp}(2.4\text{ K}) \sim 0.7$ dyn/cm^2 and $r_p \sim \xi_{\parallel}(0) \simeq 80$ Å, this gives $J_c(2.4\text{ K}) \simeq 25$ A/cm^2. For parallel vortices, using $k_p^{\parallel} \simeq 10^{-3}$ dyn/cm^2 and $r_p \sim L_J = \gamma s \simeq 5000$ Å results in $J_c^{\parallel} \simeq 2.5$ A/cm^2. The critical currents were estimated by Mota *et al.* from remnant magnetization measurements,[26] with the results $J_c^{\perp}(4\text{ K}) \simeq 250$ A/cm^2 and $J_c^{\parallel}(0) \simeq 3$ A/cm^2, in fair agreement with our estimates. The nature and concentration of the pinning sites will significantly affect k_p and J_c, and so considerable variation with the conditions of sample growth and purity is to be expected.

Just as the anisotropy of the collective effects initially seems to contradict the pinning force anisotropy ($k_p^{\perp} \gg k_p^{\parallel}$), it also seems surprising that the onset of reversible

(nonhysteretic) behavior in $\chi'(H)$ occurs at much lower fields in the perpendicular orientation (Fig. 6). Furthermore, the peak in the imaginary part $\chi''(H)$, which is related to dissipation, is also larger in perpendicular fields. These results taken together seem to indicate that flux creep occurs much more easily in perpendicular fields, despite the much weaker *linear* (small amplitude) restoring force for Josephson vortices. This is in agreement with the measurements of the creep rate $-\partial \ln M/\partial \ln t$ of Mota *et al.*[26] They found that the creep rate was roughly a factor of three *smaller* for parallel fields at all temperatures. There is thus a complicated interplay between the pinning force constant, the length scale r_p, collective effects, and thermal effects in determining the magnetic behavior.

V. LOCK-IN EFFECT AND ANGULAR DEPENDENCE

Figures 10(a) and 10(c) show the screening strength $-4\pi\chi'(H)$ for **H** applied at an angle θ with the layers, for a series of angles from $\theta = 0^0$ (**H** parallel to the layers) to $\theta = 64°$, and for temperatures of 2.4 and 4.2 K. A striking nonmonotonic behavior is observed, as reported in Ref. 24. Regardless of the angle, the screening strength initially decays in exactly the same way as for parallel fields ($\theta = 0$). At an angle-dependent threshold field $H_{\rm th}(\theta)$, the screening at finite angles begins to deviate from the parallel field value, reaches a minimum, and then *recovers* (to nearly the zero field value for larger angles). This is extremely unusual in that increasing the field strength leads to the *enhancement* of screening, a property characteristic of superconductivity. A maximum of the screening occurs at a field roughly double that of the screening minimum, and χ' decays monotonically with H above this.

We repeat here the interpretation of these features in terms of the lock-in effect, first given in Ref. 24, with reference to Fig. 11. A magnetic field applied at an angle initially enters the sample only in the parallel direction, and the vortex lattice consists only of weakly pinned Josephson vortices. The susceptibility therefore decays rapidly with field, just as for $\theta = 0$ [Fig. 11(a)], due to a large vortex penetration depth λ_y from the edges of the sample. At the threshold field $H_{\rm th}$, the flux lines unlock from the layers. Although the vortex density continues to increase, the rapid increase in the pinning strength due to the proliferation of strongly pinned 2D normal cores causes the reduction of λ_y and the recovery of screening [Fig. 11(b)]. Finally, well above the lock-in threshold, **B** $\|$ **H** [Fig. 11(c)]. Both penetration depths λ_y and λ_z increase with field as the vortex density continues to increase, leading to the monotonic decrease of the screening.

In Figs. 10(b) and 10(d), the data of Figs. 10(a) and 10(c) are plotted against the perpendicular field component $H_\perp = H\sin\theta$. The scaling of the lock-in threshold with the perpendicular field component is immediately obvious when the data are plotted in this way. Another feature of the data, not described in Ref. 24, is also apparent: The susceptibility is determined only by $H_\perp$ for

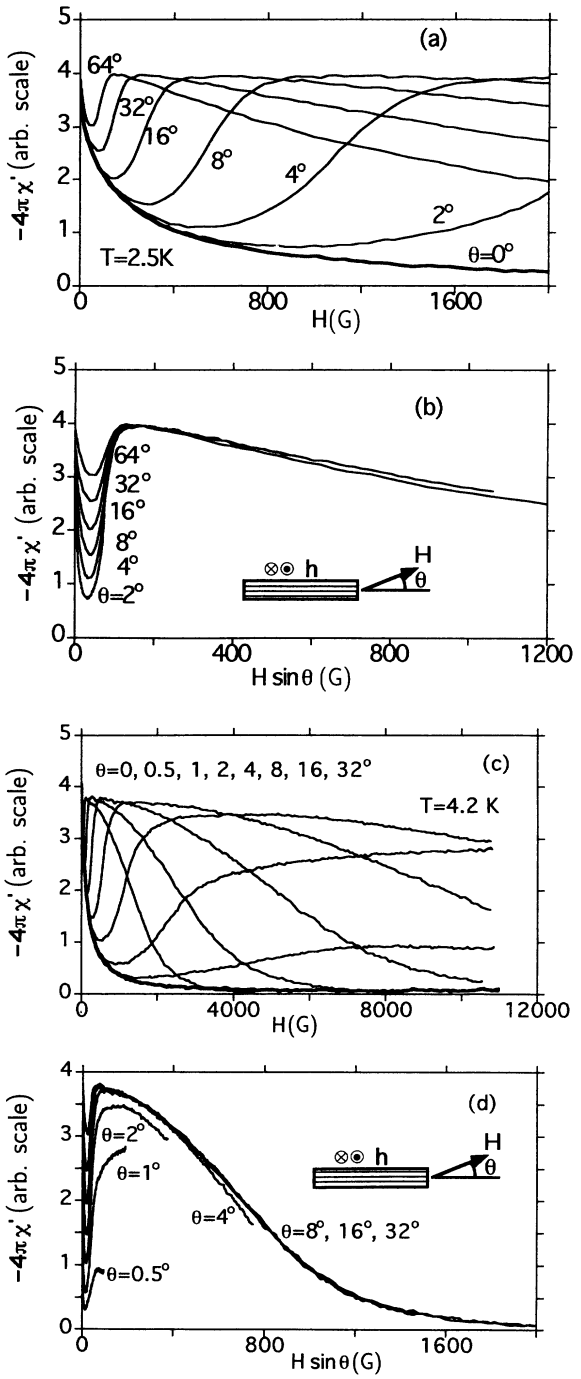

FIG. 10. $\chi'(H)|_\theta$ data sets at temperatures of 2.4 K (a),(b), and 5 K (c),(d), plotted against both the total field and the perpendicular field component. Insets show the experimental geometry.

field strengths well above the lock-in threshold and for sufficiently large angles, $\theta \gtrsim 5°$–$10°$. That is, the screening is the same as would occur for a field of total strength $H_\perp$ applied normal to the layers, $\theta = 90°$. (The failure of this scaling at small angles is obvious in the 4.2 K data; this is not seen in the 2.4 K data because the smallest angle studied was $\theta = 2°$, and the maximum value of $H_\perp$ was 2000 sin 2° = 70 G.) The scaling behavior in-

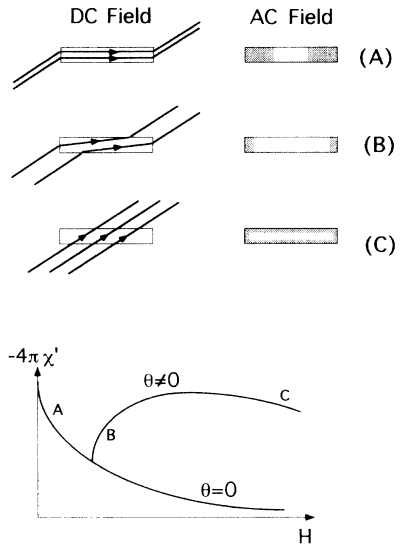

FIG. 11. Schematic representation of the dc field configuration (left) and the ac field distribution (right), in the lock-in state (A), just above the lock-in transition (B), and well above the transition (C), corresponding to the labeled portions of the curves at bottom.

cludes the changes in the form of the field dependence which were associated with a temperature-driven transition from single-vortex to collective pinning (Sec. IV).

Scaling of the in-plane resistivity[61] and critical current[62] with $H_\perp$ has previously been observed in the cuprates, and was initially taken as evidence for a purely two-dimensional model, in which $H_\perp$ leads to the creation of perpendicular vortices and the parallel field component $H_\parallel$ passes freely between the layers, without creating vortices.[2] A purely 2D model is clearly inappropriate to describe our experiments, since we observe the effects of Josephson vortex motion in parallel fields. The susceptibility is determined by both penetration depths λ_z and λ_y, and the breakdown of scaling at small angles is due to the easy motion of slightly tilted vortices and the resulting large penetration depth λ_y. We therefore interpret the scaling with $H_\perp$ as being due to scaling of the vortex penetration depth λ_z for *tilted* vortices, together with a negligible contribution of λ_y to ac field penetration in the range of fields and angles for which scaling is observed.

As discussed in Sec. II, the vortex penetration depth in the z direction λ_v should have the angular dependence $\lambda_v^2 \sim B\sin^2\phi/k_p(\phi)$. The observed scaling therefore suggests that the pinning constant for tilted vortices in ET obeys $k_p(\phi) \sim \sin\phi$ for large ϕ. This is exactly what one would expect for a vortex consisting of a tilted stack of coupled pancake vortices, since the line density of 2D normal cores is proportional to $\sin\phi$, and k_p is the pinning force *per unit length.* The Josephson core segments only exist for[15] $\phi \lesssim \tan^{-1}(1/\gamma) \simeq 0.3°$, and simply provide the limiting pinning force as $\phi \to 0$. We therefore propose the simple expression

$$k_p(\phi) = k_p^\parallel + k_p^\perp \sin\phi, \tag{5.1}$$

for tilted vortices moving parallel to the layers and transverse to the vortex axis. The second term dominates as long as $\phi \geq k_p^\parallel/k_p^\perp \simeq 0.1°$, leading to the observed scaling of λ_z. The observation of collective pinning effects in the scaled susceptibility at 4.2 K indicates that the interactions between pancake vortices affect their pinning in a way which depends only on the two-dimensional density of pancake vortices, not on the tilt angle. In other words, the coefficient $k_p^\perp$ in Eq. (5.1) depends only $B_\perp$. Besides being consistent with the observed scaling of λ_z, Eq. (5.1) can be used to construct a simple phenomenological model which qualitatively reproduces many of the features of our data, including the nonmonotonic behavior associated with the lock-in effect; we describe this model in the Appendix.

The lock-in effect has a simple theoretical explanation.[15–19] Keeping the flux lines locked to the layers causes the distortion of the magnetic field around the sample and raises energy of interaction between the sample and the external field. On the other hand, allowing the flux lines to unlock leads to the introduction of pancake vortices or vortex "kinks" wherever a flux line crosses a superconducting layer, and this raises the internal energy of the superconductor. When these energies are balanced against each other, it is found that the lock-in state is favorable as long as the perpendicular field component $H_\perp = H\sin\theta$ is below a threshold value,[15]

$$H_\perp < H_J = H_{c1}^\perp \frac{\ln(\gamma s/\xi_\parallel)}{\ln(\lambda_\parallel/\xi_\parallel)} \tag{5.2}$$

(as long as $\gamma s < \lambda_\parallel$, which seems to be true for ET). $H_{c1}^\perp$ is the perpendicular lower critical field. The lock-in effect does not occur in the anisotropic Ginzburg-Landau model because the normal core is present for *all* orientations. The core contribution to the internal energy is quadratic ($\sim \phi^2$) in the AGL model, while for Josephson coupled layers it is linear ($\sim |\phi|$) and there is a cusp in the energy at $\phi = 0$. The lock-in effect and the large anisotropy of k_p thus have a common origin, in the absence of the normal core for Josephson vortices.

Depending on the values of γ and $\lambda_\parallel$ used in Eq. (5.2), and with $\xi_\parallel(0) = 80$ Å, Eq. (5.2) gives $H_J \sim (0.7$–$0.95)H_{c1}^\perp$ for ET. We showed in Ref. 24 [Fig. 4(b)] that our $H_J(T)$ has a similar magnitude and temperature dependence to the demagnetization-corrected lower critical field $H_{c1}^\perp(T)$ measured by Mota *et al.*[26] When properly corrected for the demagnetization factor of our sample, our $H_J(T)$ actually *exceeds* the lower critical field of Mota *et al.* by about 20%. However, the definition of the threshold field used in Ref. 24 corresponds roughly to the minimum of screening, and is somewhat arbitrary. Defining $H_{\rm th}$ by the first measurable deviation of $\chi'(H)|_\theta$ from $\chi'(H)|_{\theta=0}$ would give a value nearly a factor of 2 smaller. We can at most say that our $H_J(T)$ and the $H_{c1}^\perp(T)$ of Mota *et al.* agree to better than a factor of 2. We also note that $H_{c1}^\perp(0) \simeq 300$ G in Ref. 26, while the Ginzburg-Landau expression $H_{c1}^\perp = (\Phi_0/4\pi\lambda_\parallel^2)[\ln(\lambda_\parallel/\xi_\parallel) + 0.5]$ gives $H_{c1}^\perp \sim 12$ G for ET. This, and the anomalous positive curvature in the temperature dependence, leads us

to the conclusion that both our H_J and the $H_{c1}^{\perp}$ measurements of Mota *et al.* are significantly enhanced at low temperatures due to pinning.

VI. NONLINEARITY IN PARALLEL FIELDS

We have studied the linearity of the real and imaginary parts of the susceptibility by varying the ac field amplitude h, with $f = 2.5$ kHz. In the presence of a magnetic field perpendicular to the layers, we find that both χ' and χ'' are linear for a factor of 10 increase in h. When h is reduced by a factor of 10, both χ' and χ'' appear to be linear, but the poor signal to noise ratio did not permit an unambiguous result for χ''.

A dramatic nonlinearity is observed in the absence of a dc field or whenever the internal field **B** is parallel to the layers. In Fig. 12(a), we show $-4\pi\chi'(T)$ with $H = 0$, for different values of h. The screening response is linear for $h \leq 0.3$ G, but the susceptibility is strongly suppressed for $h = 1$ G and 4.7 G. In fact, in the temperature range $T \sim 4$–6 K , increasing h from 1 to 4.7 G suppresses the susceptibility by about a factor of 4.7, indicating that the induced ac magnetic moment has saturated [Fig. 12(b), which shows $m = \chi h$ vs h]. Figure 12(c) shows the dc field dependence of χ' for a drive amplitude of $h = 4.7$ G at $T = 3.3$ K, for angles of $\theta = 0°$ and $\theta = 10°$. The points are data, and the solid line is a fit of Eqs. (2.1) and (4.1) to the $\theta = 0$ data. The fitting parameters are $\lambda_\perp = 910$ μm and $k_p^{\parallel} = 1.7 \times 10^{-4}$ dyn/cm^2. Thus the field-dependent part of the penetration depth obeys $\lambda \sim \sqrt{B}$ in both the linear and nonlinear regimes, for **B** parallel to the layers. When the perpendicular field component penetrates above the lock-in threshold, the absolute value of the screening $-4\pi\chi'$ recovers to values ~ 0.5, typical of the linear (low h) regime. In other words, the strong nonlinearity only occurs in the *absence* of perpendicular flux.

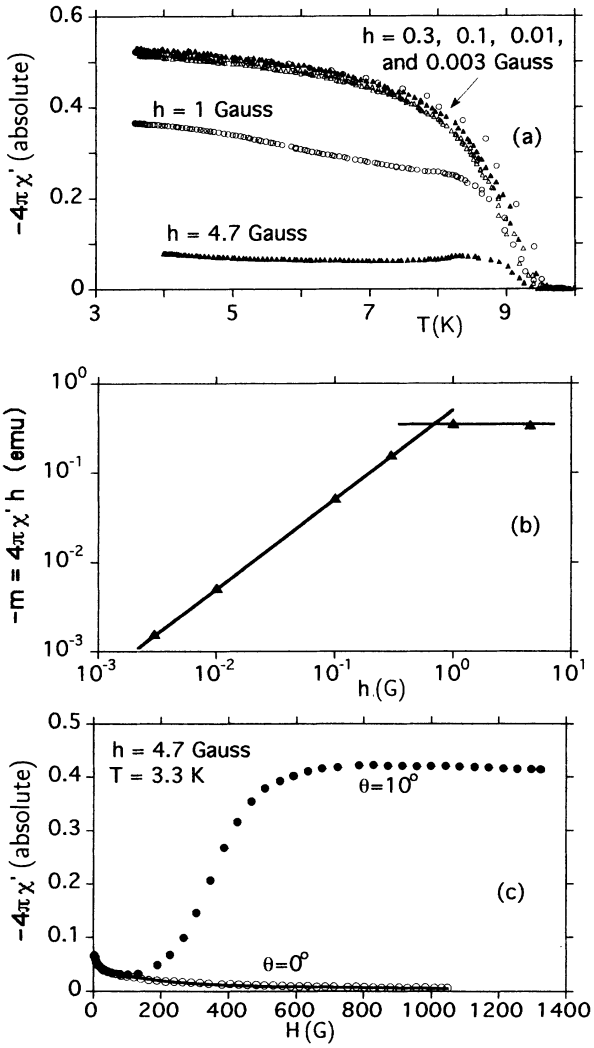

FIG. 12. Nonlinear effects. (a) $\chi'(T)$ with $H = 0$, for various h (ac field amplitude). Geometry is as shown in Fig. 5(b). (b) The induced ac magnetic moment m appears to saturate at $h \sim 0.6$ G. χ' is taken from (a) with $T = 4$ K. (c) The nonlinearity persists in the lock-in state, but the penetration of the perpendicular field component restores linear response.

Two explanations immediately come to mind. First, the screening response should be limited by the interlayer critical current J_0, and become nonlinear for ac fields larger than that given by $\nabla \times \mathbf{h} \sim h_{\rm NL}/\lambda_\perp = 4\pi J_0/c$, or $h_{\rm NL} = 4\pi J_0 \lambda_\perp/c$. This explanation is appealing because of the observed saturation of the ac magnetization above the threshold. However, the penetration of the perpendicular field component largely restores the linear response, and this would imply that the interlayer supercurrent can exceed J_0 in the presence of perpendicular flux. Also, using the relationship $J_0 = c\Phi_0/8\pi^2 s\lambda_\perp^2$ for a layered material, $h_{\rm NL} = \Phi_0/2\pi s\lambda_\perp \simeq 10$ G, about factor of 20 larger than the observed threshold. These observations argue against this being the correct explanation for the nonlinearity.

The reduction of the nonlinearity by perpendicular flux suggests another possibility: that the ac field exceeds the lower critical field parallel to the layers, leading to the introduction of weakly pinned Josephson vortices and antivortices in alternate parts of the ac field cycle. The motion of these in response to the ac field then leads to the reduction in screening, while the introduction of perpendicular flux either damps their motion or prevents ac-field-induced nucleation of Josephson vortices from occurring. Measured values of the parallel lower critical field, from dc magnetization experiments, are $H_{c1}^{\parallel} = 0.6$ G at $T = 5$ K (Ref. 50) and an upper limit of $H_{c1}^{\parallel} < 0.5$ G,[26] while the value calculated from the formula of Clem *et al.* is 0.06 G.[64] Thus it is quite plausible that an ac field of amplitude $h \geq 1$ G would lead to the introduction of Josephson vortices.

Beyond this, the details of the mechanism for the nonlinearity are unclear at present. From Fig. 7, it can be seen that a parallel dc field of several hundred gauss is needed to produce a suppression of $-4\pi\chi'$ equivalent to that achieved by an ac field of 4.7 G, implying that a very high net density of vortices must be present for the above explanation to work. This is presumably determined by the balance between vortex nucleation at the edges of the sample, and vortex-antivortex annihilation

in the bulk. The picture is further complicated by the fact that a field of only a few tenths of a gauss is sufficient to induce interlayer currents comparable to the depinning critical current, $J_c^{\parallel} \sim 3$ A/cm^2 (Sec. IV B), so that this should play a role as well. The frequency dependence in the nonlinear (large h) regime is still weak, however, comparable to that observed in the linear regime, and this is inconsistent with viscosity-limited motion of completely depinned vortices. Thus while the nonlinearity provides another striking demonstration of the qualitatively different behavior observed when the vortices are parallel to the layers, this effect is not well understood at present.

VII. CONCLUSIONS

We have described ac susceptibility measurements on a single crystal of (BEDT-TTF)$_2$Cu(NCS)$_2$ which provide strong evidence for the existence of Josephson vortices in this material, and clearly show that their properties are different than those of tilted or perpendicular vortices. The lock-in effect and the anomalously weak pinning force for Josephson vortices are direct consequences of the absence of the usual normal core region. The pinning force anisotropy is on the order of $k_p^{\perp}/k_p^{\parallel} \sim 500$, and the force constants could be related to the appropriate energy and length scales for Abrikosov and Josephson vortex cores, and to the observed depinning critical currents. $k_p^{\parallel}$ is field independent up to $H = 3$ kG at all temperatures, while $k_p^{\perp}$ decreases with field (except at $T = 2.4$ K). We have attributed these observations to single-vortex pinning and collective pinning, respectively. This is consistent with theoretical calculations which show that the parallel field shear modulus C_{66}^{e} is a factor of $\sim \gamma^3 \simeq 10^7$ weaker than for perpendicular fields, due to the anisotropic structure of the vortices and the vortex lattice. The susceptibility scales with the perpendicular field component $H_{\perp}$ for sufficiently large fields and angles, showing that the dynamics of tilted vortices are determined by the pinning and interactions of the 2D pancake vortices. We have also observed a highly nonlinear response to the ac field in the lock-in state, with a threshold of $h \sim 0.5$ G, but linear response is largely restored when the flux lines unlock from the layers. Finally, we have measured the Josephson penetration depth to be $\lambda_{\perp}(T = 5\ \mathrm{K}) \simeq 200\ \mu$m, consistent with the result $\gamma \geq 200$ from torque measurements.

Our experiments show that motion of Josephson vortices in the direction *parallel* to the layers can have an enormous effect on the electromagnetic properties of a layered superconductor, and that it is the interaction of Josephson vortices with interlayer currents which is most significant. Several studies of the angular dependence of in-plane transport properties have shown anomalous enhancements of the resistance near the parallel orientation,[61,65] and we suggest that these may be due in part to interlayer currents which occur near cracks or twin boundaries. There have been proposals to utilize intrinsic pinning in applications of high T_c superconductivity, e.g., by winding an oriented polycrystalline tape into a solenoid with the copper oxide planes tangent to the surface, so that the field will be parallel to the layers.[66] This orientation gives the minimum resistance even without intrinsic pinning. The effectiveness of such an application might be limited by the occurrence of stray interlayer currents and the resulting Josephson vortex motion, and a detailed understanding of the nature of Josephson vortex pinning and the type of defects responsible is therefore potentially of some practical interest.

It is hoped that this work will stimulate further research on the properties and behavior of Josephson vortices. Besides the absence of the normal core and the weak and highly anisotropic elastic forces, vortex motion and fluctuations are essentially restricted to one dimension by intrinsic pinning, and entanglement is impossible in the absence of thermally activated kinks. All of these factors should have a significant effect on the statistical mechanics of Josephson vortices, and the consequences for the controversial issue of the vortex lattice melting or vortex glass phase transition[38] have recently begun to be explored experimentally.[67]

(BEDT-TTF)$_2$Cu(NCS)$_2$ is an excellent candidate for such experiments, and in general for further work on vortices in layered superconductors. Not only is $\xi_{\perp} < s$ over virtually the entire temperature range [for $T/T_c < \sqrt{1-(\xi_{\parallel}/\gamma s)^2} = 0.9996$], but the entire (H,T) phase diagram is experimentally accessible, since= $H_{c2}^{\parallel}(0) \simeq 20$ T. Large single crystals are easily grown, and the pinning is extremely weak, allowing the effects we report here to be observed so readily by ac susceptibility. An important issue for future work on this and other organic superconductors is the characterization of the defects responsible for pinning.

ACKNOWLEDGMENTS

The authors thank L. Bulaevskii, M. Coffey, D. Huse, V. Kogan, M. Ledvij, and N.P. Ong for helpful discussions at various points in this work. This research was supported by NSF Grant No. DMR 92-04581.

APPENDIX: A SIMPLE MODEL FOR THE SUSCEPTIBILITY

Beyond simply providing an explanation for the scaling of $\lambda_z(H_{\perp})$ for tilted vortices, Eq. (5.1) can also be used to calculate λ_y. By combining Eq. (5.1) with Eq. (2.3) for $\chi(\lambda_y/L_y, \lambda_z/L_z)$, and a simple relationship between B and H which at least qualitatively describes the lock-in effect, we can construct a simple phenomenological model which captures most of the essential features of the data. With reference to Eqs. (2.7) and (5.1), and to Figs. 2(b), 3(b), and 13(a), the penetration depths from the edges and surfaces of the sample (λ_y and λ_z, respectively) are

$$\lambda_y^2 = \frac{B\Phi_0 \cos^2\phi}{4\pi(k_p^{\parallel} + k_p^{\perp}\sin\phi)} + \lambda_{\perp}^2 \qquad \text{(A1)}$$

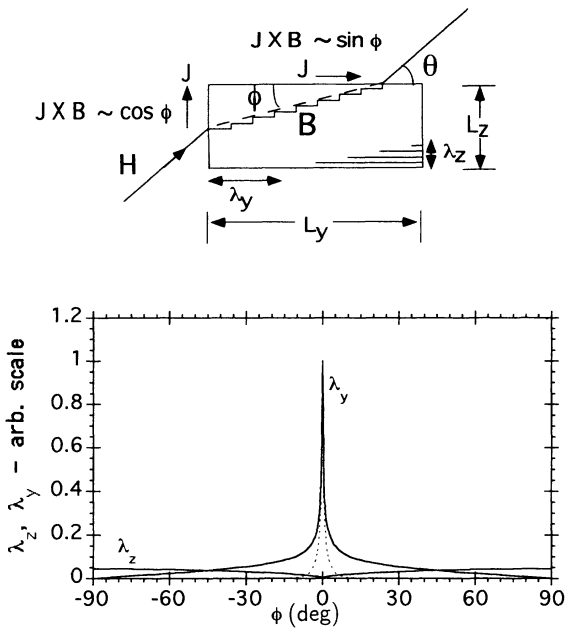

FIG. 13. (a) Geometry for the model calculation of the susceptibility. (b) Angular dependence of the penetration depths λ_z and λ_y, with B fixed. Vertical scale is arbitrary, but is the same for both penetration depths. Dashed lines show the effect of the cutoff on $\lambda_y(\phi)$; see the Appendix.

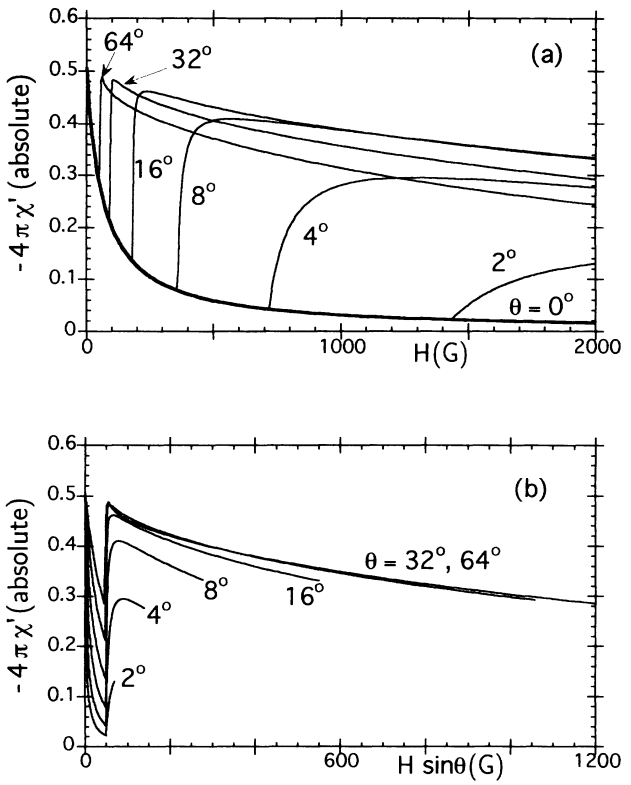

FIG. 14. Results of model calculation of susceptibility, plotted against (a) the applied field strength H and (b) the perpendicular field component $H_\perp$. Compare to Fig. 10(a) and (b), respectively.

and

$$\lambda_z^2 = \frac{B\Phi_0 \sin^2\phi}{4\pi(k_p^{\parallel} + k_p^{\perp}\sin\phi)} + \lambda_{\parallel}^2. \qquad \text{(A2)}$$

The angular dependence of λ_y and λ_z (with B=const, and $\lambda_\perp = \lambda_{\parallel} = 0$ for simplicity) is shown in Fig. 13(b). The penetration depth anisotropy in fixed field, $\lambda_y^{\max}/\lambda_z^{\max} = \sqrt{k_p^{\perp}/k_p^{\parallel}} \simeq \sqrt{500} = 22$, is much larger than the typical sample aspect ratio $L_y/L_z \simeq 5$. We do not show experimental data for the angular dependence of χ' at fixed field in this paper, but Fig. 3 in Ref. 24 shows that there is a deep minimum in $-4\pi\chi'(\theta)|_H$ at $\theta = 0°$, due to the peak in $\lambda_y(\phi)$, and the half width $\theta_{\rm th}$ of the minimum depends on H as $H\sin\theta_{\rm th} = H_J(T)$ =const. The angular dependence data also scale with $H_\perp$ for $H_\perp \gg H_J$ (not shown).[40]

In order to model the lock-in effect, we need to know the relationship between **B** and **H** near the transition. Although this has recently been studied in detail by Koshelev,[63] pinning of the 2D vortices will cause significant deviations from the equilibrium behavior, and $H_\perp$ will probably penetrate as in the Bean critical state model. In the absence of a detailed model for this, and in the interest of simplicity, we use the approximation that $B_{\parallel} = H_{\parallel}$ for all H, while $B_\perp = 0$ for $H_\perp < H_J$ and $B_\perp = H_\perp - H_J$ for $H_\perp > H_J$. This is certainly not accurate, but at least qualitatively models the behavior near the lock-in threshold and gives the correct limiting behavior ($B = H$) for $H_\perp \gg H_J$.

Equation (2.3), when combined with Eq. (5.1) for $k_p(\phi)$, Eqs. (A1) and (A2) for λ_y and λ_z, and the above approximation for $\mathbf{B}(\mathbf{H})$, gives the results shown in Fig. 14(a). This is meant to simulate the $T = 2.4$ K data of Fig. 10(a). The parameters used are $H_J = 50$ G, $k_p^{\parallel} = 10^{-3}$ dyn/cm^2, $k_p^{\perp} = 1$ dyn/cm^2, $L_z = 0.015$ cm, $L_y = 0.08$ cm, $\lambda_\perp = 0.02$ cm, and $\lambda_{\parallel} = 0$. The results of the model are plotted against $H_\perp$ in Fig. 14(b). This points out the most serious deficiency of the model, that the scaling behavior is not observed until about $\theta = 32°$; for smaller angles, the scaled screening strength $-4\pi\chi'$ is less than the value for perpendicular fields. Because λ_z clearly scales with $H_\perp$ for large ϕ in the model, this must occur because the model predicts much larger values of λ_y for large ϕ than are actually occurring in the experiment. Multiplying the vortex term in Eq. (A1) by a cutoff of the form $\exp(-|\phi/\phi_0|)$, with $\phi_0 \sim$ a few degrees [dashed line in Fig. 13(b)] leads to improved scaling of the model results, but this procedure is arbitrary. The reason for this discrepancy is not understood. A less serious deficiency of the model is that the recovery of screening above the lock-in threshold is much more abrupt than in the data, and this is almost certainly due to the fairly arbitrary relationship between B and H used in the model near the transition.

* Present address: IBM Research Division, Almaden Research Center, 650 Harry Road, San Jose, CA 95120-6099.
[1] John R. Clem, Phys. Rev. B **43**, 7837 (1991).
[2] P.H. Kes, J. Aarts, V.M. Vinokur, and C.J. van der Beek, Phys. Rev. Lett. **64**, 1063 (1990).
[3] L.N. Bulaevskii, M. Ledvij, and V.G. Kogan, Phys. Rev. Lett. **68**, 3773 (1992).
[4] P.H. Kes *et al.*, Phys. Rev. Lett. **67**, 2383 (1991); Qiang Li, M. Suenaga, T. Hikata, and K. Sato, Phys. Rev. B **46**, 5857 (1992).
[5] H. Safar *et al.*, Phys. Rev. Lett. **72**, 1272 (1994); H. Safar *et al.*, Phys. Rev. B **46**, 14 238 (1992).
[6] V.M. Vinokur, P.H. Kes, and A.E. Koshelev, Physica C **168**, 29 (1990).
[7] V.G. Kogan, Phys. Rev. B **24**, 1572 (1981).
[8] L.J. Campbell, M.M. Doria, and V.G. Kogan, Phys. Rev. B **38**, 2439 (1988).
[9] V.G. Kogan and L.J. Campbell, Phys. Rev. Lett. **62**, 1552 (1989).
[10] G.J. Dolan, F. Holtzberg, C. Feild, and T.R. Dinger, Phys. Rev. Lett. **62**, 2184 (1989).
[11] J.R. Clem and M.W. Coffey, Phys. Rev. B **42**, 6209 (1990).
[12] L. Bulaevskii and J.R. Clem, Phys. Rev. B **44**, 10 234 (1991).
[13] Michael Tinkham, *Introduction to Superconductivity* (Robert E. Krieger Publishing Co., Malabar, FL, 1975), pp. 178–181.
[14] S.S. Maslov and V.L. Pokrovskii, JETP Lett. **53**, 637 (1991).
[15] L.N. Bulaevskii, M. Ledvij, and V.G. Kogan, Phys. Rev. B **46**, 366 (1992), and references therein.
[16] L.N. Bulaevskii, Phys. Rev. B **44**, 910 (1991).
[17] D. Feinberg and C. Villard, Phys. Rev. Lett. **65**, 919 (1990).
[18] D. Feinberg, J. Phys. (France) III **4**, 169 (1994).
[19] D. Feinbergand and A.M. Ettouhami, Int. J. Mod. Phys. B **7**, 2085 (1993).
[20] W.K. Kwok *et al.*, Phys. Rev. Lett. **67**, 390 (1991).
[21] D.E. Farrell *et al.*, Phys. Rev. Lett. **64**, 1573 (1990).
[22] O.H. Chung, M. Chaparala, and M.J. Naughton, in *Proceedings of the VIth NYSYS Conference on Superconductivity*, Sept. 1992, Buffalo (AIP, New York, 1993).
[23] N.V. Zavaritskii and V.N. Zavaritskii, JETP Lett. **55**, 226 (1991).
[24] Paul A. Mansky, P.M. Chaikin, and R.C. Haddon, Phys. Rev. Lett. **70**, 1323 (1993).
[25] D.E. Farrell and C.J. Allen, Phys. Rev. B **42**, 8694 (1990).
[26] A.C. Mota *et al.*, Physica C **185-189**, 343 (1991).
[27] A.I. Larkin and Yu.N. Ovchinnikov, J. Low Temp. Phys. **34**, 409 (1979).
[28] G. Saito, Physica C **162-164**, 577 (1989).
[29] V.B. Geshkenbein, V.M. Vinokur, and R. Fehrenbacher, Phys. Rev. B **43**, 3748 (1991).
[30] M.W. Coffey and J.R. Clem, Phys. Rev. B **45**, 9872 (1992).
[31] A.M. Campbell, J. Phys. C **4**, 3186 (1971).
[32] M.W. Coffey and J.R. Clem, Phys. Rev. B **45**, 10 527 (1992).
[33] M.W. Coffey and J.R. Clem, Phys. Rev. Lett. **67**, 386 (1991).
[34] E.H. Brandt, Phys. Rev. Lett. **67**, 2219 (1991).
[35] E.H. Brandt, Z. Phys. B **80**, 167 (1990).
[36] Hui Wu, N.P. Ong, and Y.Q. Li, Phys. Rev. Lett. **71**, 2642 (1993).
[37] J. Kotzler *et al.*, Phys. Rev. Lett. **72**, 2081 (1994).
[38] M.P.A. Fisher, Phys. Rev. Lett. **62**, 1415 (1989); Daniel S. Fisher, Matthew P.A. Fisher, and David A. Huse, Phys. Rev. B **43**, 130 (1991).
[39] A.T. Dorsey *et al.*, Phys. Rev. B **45**, 523 (1992).
[40] Paul A. Mansky, Ph.D. thesis, Princeton University, 1993.
[41] A.P. Malozemoff, T.K. Worthington, Y. Yeshrun, and F. Holtzberg, Phys. Rev. B **38**, 7203 (1988).
[42] D.R. Harshman *et al.*, Phys. Rev. Lett. **64**, 1293 (1990); L. P. Le *et al.*, *ibid.* **66**, 655 (1991).
[43] M. Lang *et al.*, Phys. Rev. Lett. **69**, 1443 (1992).
[44] K. Holczer *et al.*, Phys. Rev. Lett. **66**, 655 (1991).
[45] K. Oshima *et al.*, J. Phys. Soc. Jpn. **57**, 730 (1988); K. Oshima *et al.*, in *The Physics and Chemistry of Organic Superconductors*, edited by G. Saito and S. Kagoshima, Springer Proceedings in Physics Vol. **51** (Springer, Berlin, 1990), p. 276.
[46] J.E. Graebner *et al.*, Phys. Rev. B **41**, 4808 (1990).
[47] K. Kanoda *et al.*, Phys. Rev. Lett. **65**, 1271 (1990).
[48] H. Schwenk, K. Andres, F. Wudl, and E. Aharon-Shalom, Solid State Commun. **45**, 767 (1983); H. Schwenk, K. Andres, and F. Wudl, *ibid.* **49**, 723 (1984).
[49] James J. Finley and Bascom S. Deaver, Solid State Commun. **36**, 493 (1980).
[50] M. Tokumoto *et al.*, Synth. Met. **27**, A305 (1988).
[51] Dong-Ho Wu and S. Sridhar, Phys. Rev. Lett. **65**, 2074 (1990).
[52] Dong-Ho Wu, C.A. Shiffman, and S. Sridhar, Phys. Rev. B **38**, 9311 (1988).
[53] L. Krusin-Elbaum, L. Civale, V.M. Vinokur, and F. Holtzberg, Phys. Rev. Lett. **69**, 2280 (1992).
[54] A. Sudbo and E.H. Brandt, Phys. Rev. Lett. **68**, 1758 (1992).
[55] E.H. Brandt, Phys. Status. Solidi B **77**, 551 (1976); J. Low Temp. Phys. **26**, 709 (1977).
[56] A.E. Koshelev and V.M. Vinokur, Physica C **173**, 465 (1991).
[57] M.V. Feigel'man, V.B. Geshkenbein, and A.I. Larkin, Physica C **167**, 177 (1990).
[58] Boris A. Malomed, Phys. Rev. B **38**, 9242 (1988).
[59] M.B. Mineev, M.V. Feigel'man, and V.V. Shmidt, Sov. Phys. JETP **54**, 155 (1981).
[60] A qualitatively similar variation of the interlayer current and phase occurs in the other junctions as well ($z = ns \neq 0$), and these should also contribute to the pinning. However, one can show using the results of Clem and Coffey (Ref. 11) that the maximum phase difference $\Delta\varphi_n$ in layer n is about $\pm 1/2|n|$, and occurs at a distance $y_n \simeq \pm nL_J$ from the center ($y = 0$). The contribution of junction n to the restoring force $k_p^{\parallel}$ should therefore fall off roughly as $1/|n|^2$, and the central junction ($n = 0$) should dominate the pinning.
[61] Y. Iye, T. Tamegai, and S. Nakamura, Physica C **174**, 227 (1991); Y. Iye, T. Terashima, and Yoshichika Bando, *ibid.* **177**, 393 (1991).
[62] Qi Li *et al.*, Phys. Rev. Lett. **69**, 2713 (1992).
[63] A.E. Koshelev, Phys. Rev. B **48**, 1180 (1993).
[64] John R. Clem, Mark W. Coffey, and Zhidong Hao, Phys. Rev. B **44**, 2732 (1991).
[65] R. Fastampa, M. Giura, R. Marconi, and E. Silva, Europhys. Lett. **18**, 75 (1992).
[66] P.H. Kes, Nature **350**, 192 (1991).
[67] W.K. Kwok *et al.*, Phys. Rev. Lett. **72**, 1088 (1994).

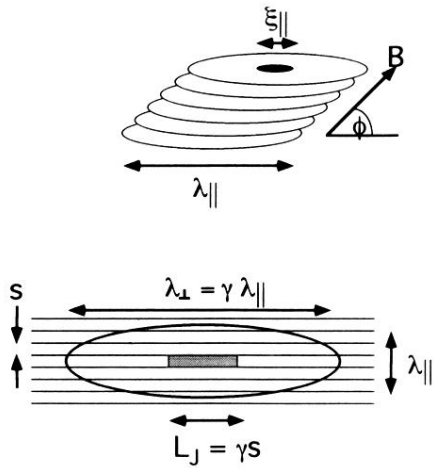

FIG. 1. Top: a tilted flux line consists of a stack of two-dimensional Abrikosov "pancake" vortices, each of which contains a normal core (dark area). The vortex makes an angle ϕ with the layers. Bottom: structure of a Josephson vortex, viewed along the field direction. The superconducting order parameter maintains its full value everywhere on the layers. The Josephson "core" (shaded area) is the region in which the tunneling current is comparable to the Josephson critical value J_0 and has width $L_J = \gamma s > \xi_{\|}$.

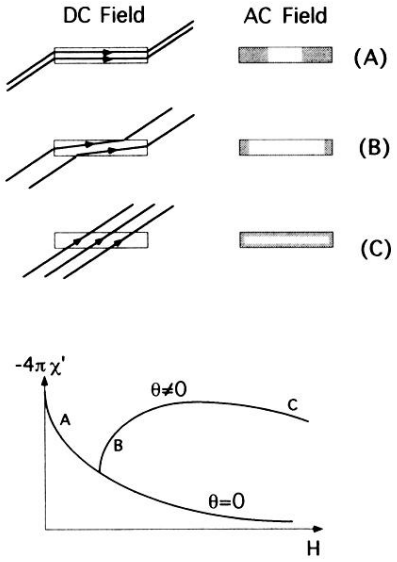

FIG. 11. Schematic representation of the dc field configuration (left) and the ac field distribution (right), in the lock-in state (A), just above the lock-in transition (B), and well above the transition (C), corresponding to the labeled portions of the curves at bottom.

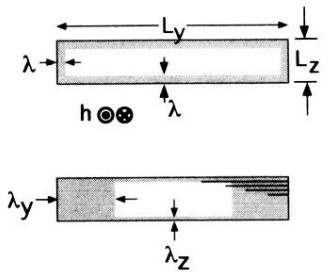

FIG. 2. Field penetration (shaded areas) in isotropic and anisotropic superconductors with rectangular cross sections. (a) For an isotropic superconductor, field penetration from the edges can be ignored if $L_y \gg L_z$. (b) This is not the case in an anisotropic superconductor if $\lambda_y/L_y \gg \lambda_z/L_z$.

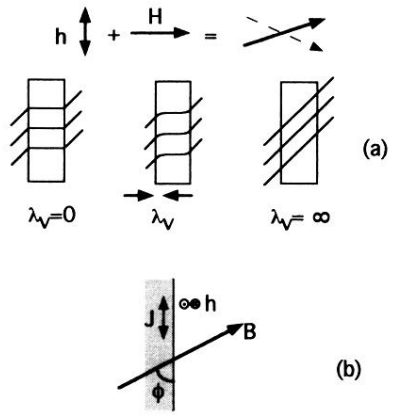

FIG. 3. (a) Relationship between ac field penetration and flux line pinning. The total external field $\mathbf{H} + \mathbf{h}$ executes a small amplitude tilting motion (top). Left: rigidly pinned flux lines: $\mathbf{B} = \mathbf{H}$ inside while $\mathbf{B} = \mathbf{H} + \mathbf{h}$ outside, and so $\chi_{ac} = -1/4\pi$. Right: if there are no forces opposing flux line motion, then $\mathbf{B} = \mathbf{H} + \mathbf{h}$ inside the sample and $\chi_{ac} = 0$. Center: in the general case, pinning forces lead to a vortex contribution λ_v to the ac penetration depth. (b) Geometry for discussion of angular dependence of λ_v.